# Face-to-Face Stacks of Trinuclear Gold(I) Trihalides with Benzene, Hexafluorobenzene, and Borazine: Impact of Aromaticity on Stacking Interactions

Athanassios C. Tsipis* and Alexandros V. Stalikas

Laboratory of Inorganic and General Chemistry, Department of Chemistry, University of Ioannina, 451 10 Ioannina, Greece

Ⓢ *Supporting Information*

ABSTRACT: The interplay of electrostatics, charge transfer, and dispersion forces contributing to the interaction energies in 1:1, 1:2, and 2:1 binary stacks of the c-$Au_3(\mu_2$-$X)_3$ (X = F, Cl, Br, I) clusters with benzene, hexafluorobenzene, or borazine were investigated by employing a multitude of electronic structure computational techniques. The molecular and electronic structures, stabilities, bonding features, and magnetotropicity of $[c$-$Au_3(\mu_2$-$X)_3]_n(L)_m$ (X = halide; L = C_6H_6, C_6F_6, $B_3N_3H_6$; n, $m \leq 2$) columnar binary stacks have been investigated by DFT calculations employing the M05-2X functional. The novel binary

stacks could be considered as the building blocks of extended columnar supramolecular assemblies formulated as $\{[c$-$Au_3(\mu_2$-$X)_3](C_6H_6)\}_\infty$, $\{[c$-$Au_3(\mu_2$-$X)_3]_2(C_6F_6)\}_\infty$, and $\{[c$-$Au_3(\mu_2$-$X)_3](B_3N_3H_6)_2\}_\infty$. In all binary stacks, with a few exceptions, the plane of the alternating c-$Au_3(\mu_2$-$X)_3$ and L (C_6H_6, C_6F_6, $B_3N_3H_6$) stacking participants adopt an almost parallel face-to-face (**pff**) orientation. The observed trends in the intermolecular distances R in the $[c$-$Au_3(\mu_2$-$X)_3]_n(L)_m$ (X = halide; L = C_6H_6, C_6F_6, $B_3N_3H_6$; n, $m \leq 2$) columnar binary stacks are explained by the diverse intermolecular interactions characterizing the stacks, since the three ligands L and the c-$Au_3(\mu_2$-$X)_3$ cyclic trinuclear clusters (CTCs) exhibit diverse physical properties being important determinants of the intermolecular interactions (consisting of covalent, electrostatic, and dispersion forces). The properties considered are the zz tensor components of quadrupole moment, Q_{zz}, polarizability, α_{zz}, nucleus-independent chemical shift, $NICS_{zz}(1)$, along with the molecular electrostatic potential, MEP(0), and surface area (S). Energy decomposition analysis (EDA) at the revPBE-D3/TZ2P level revealed that the dominant term in the stacking interactions arises mainly from dispersion and electrostatic forces, while the contribution of covalent interactions are predicted to be small. On the other hand, charge decomposition analysis (CDA) illustrated very small charge transfer from the L stacking participants toward the c-$Au_3(\mu_2$-$X)_3$ clusters. Excellent linear correlations of the interaction energy, ΔE_{int}, and its components (ΔE_{disp}, ΔE_{elstat}, ΔE_{orb}, and ΔE_{Pauli}) with calculated physical properties related to dispersion, covalent, and electrostatic forces have been established. The most important finding is the excellent linear relationship between ΔE_{int} and the $NICS_{zz}(1)$ magnetic criterion of aromaticity, indicating that ΔE_{int} is also affected by the coupling of the induced magnetic fields of the interacting stacking participants. The magnetotropicity of the binary stacks evaluated by the $NICS_{zz}$-scan curves indicated an enhancement of the diatropicity in the space between the interacting inorganic and organic rings, probably due to the superposition of the diamagnetic ring currents of the interacting ring systems. The energy splitting in dimer (ESID) model was employed to estimate the charge transport of electrons and holes between the ligands L and the $[c$-$Au_3(\mu_2$-$X)_3]$ clusters in $[c$-$Au_3(\mu_2$-$X)_3](L)$ 1:1 binary stacks.
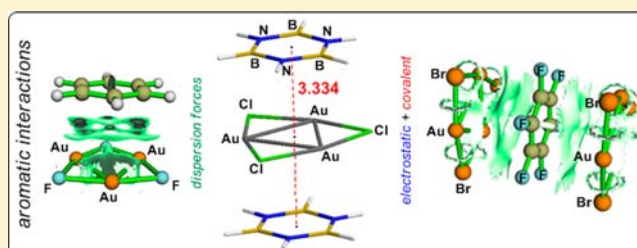
1. INTRODUCTION

Noncovalent interactions between aromatic rings play a critical role across a broad range of disciplines, from materials chemistry to molecular biology, and are vital tools in the realm of supramolecular chemistry.[1] Because aromatic–aromatic interactions are ubiquitous in nature, a large body of experimental and theoretical work has been done investigating the nature of arene–arene interactions in a vast number of organic aromatics and biomolecules.[1d,2] Model systems have also been employed to investigate the nature and significance of aromatic interactions as molecular recognition elements in biological and nonbiological systems. However, to the best of our knowledge, both experimental and theoretical studies of the nature and significance of aromatic interactions between "all-metal" and

organic aromatics are very limited. Synthesis of the discrete metal monolayer sandwich compounds $[Pd_3(C_7H_7)_2Cl_3][PPh_4]$ and $[Pd_5(naphthacene)_2(toluene)][B(Ar_f)_4]_2$, with $B(Ar_f)_4 = B[3,5$-$(CF_3)_2C_6H_3]_4$, has been reported in 2006.[3] $[Pd_3(C_7H_7)_2Cl_3]^{2+}$ is a tripalladium complex capped by chlorines between two cycloheptatrienyl ligands, while $[Pd_5(naphthacene)_2]^{2+}$ is a pentapalladium sheet with a triangle-trapezoid geometry between two naphthacene rings. Both compounds have been studied employing DFT methods. Discovery of the Pd compounds has opened a new field in the search of other metal elements that can be used in the monolayer metal sandwich chemistry, since these

molecular systems can be the building blocks of bulk systems like unsaturated hydrocarbons adsorbed on metallic surfaces.[3] The existence of the sandwich $[Au_3Tr_2Cl_3]^{2+}$ (Tr = tropylium) compound formed upon intercalation of the *cyclo*-Au_3Cl_3 cluster, representing a gold monolayer sheet, between two cyclo-heptatrienyl cations, has been predicted using ab initio and DFT calculations.[4] Recently, DFT has been employed by Cundari et al.[5] to assess the π acidity and π basicity of metallorganic trimetallic macromolecular complexes formulated as *cyclo*-$[M_3(\mu$-L$)_3]$ (M = Cu, Ag, Au; L = carbeniate, Cb, imidazolate, Im, pyridiniate, Py, pyrazolate, Pz, triazolate, Tz). The π basicity of the *cyclo*-$[M_3(\mu$-L$)_3]$ clusters depends on the nature of the bridging ligand following the trend *cyclo*-$[M_3(\mu$-Py$)_3]$ > *cyclo*-$[M_3(\mu$-Cb$)_3]$ > *cyclo*-$[M_3(\mu$-Pz$)_3]$ > *cyclo*-$[M_3(\mu$-Tz$)_3]$. It was also predicted that the order of basicity is Au > Cu > Ag. Moreover, electron-donating substituents (such as CH_3) on the bridging ligands produce strong π-basic trimers, while electron-withdrawing substituents (such as CF_3) produce strong π-acidic trimers. Very recently, we reported the molecular and electronic structure, stability, bonding features, magnetotropicity, and absorption spectra of novel benzene–trinuclear copper(I) and silver(I) trihalide columnar binary stacks.[6]

It is well established that gold(I) exhibits a remarkable tendency to form either bare or ligand-stabilized polynuclear clusters based on Au(I)−Au(I) interactions of strength comparable to that of the strongest hydrogen bonds or the weakest covalent bonds (5−15 kcal/mol).[7−10] Coordination of gold metal atom to other gold atoms has been mainly attributed to the so-called "aurophilicity" phenomenon, first introduced by Schmidbaur[11] to explain the Au−Au 'contracted' distances, ranging between 3.0 and 3.6 Å. Extensive experimental and theoretical studies demonstrated that aurophilicity originates by relativistic and correlation effects.[12] Particularly abundant are the cyclic trinuclear complexes (CTCs) of gold(I), involving three-membered metallic rings with triangular arrangement of the metal atoms. These clusters exhibit a wide range of properties relevant to fundamental as well as applied areas of research such as metallophilic interactions, metalloaromaticity, supramolecular chemistry, π-acid/π-base properties, and optoelectronic devices.[13] Of particular importance is the ability of the trinuclear Au(I) complexes to act as π-acids/π-bases which upon interaction with various arenes form extended supramolecular stacks with intriguing luminescence properties,[13a] rendering them as potential candidates for optoelectronics applications. Burini et al.[7] reported the synthesis and structures of cyclic trinuclear gold(I) clusters which form supramolecular assemblies even with a perfect columnar crystal packing. The $\{Au_3(CH_3N{=}COCH_3)_3\}$ gold(I) CTC has been reported[13b] to form deeply colored charge-transfer stacks upon interaction with nitro-9-fluorenones. Small organic electron acceptors such as C_6F_6 and TCQN have been reported[13c] to interact with electron-rich Au(I) CTCs forming supramolecular assemblies exhibiting infinite linear chains. Interestingly, C_6F_6 is intercalated between two Au(I) CTCs, disrupting aurophilic interactions and yielding 1:1 adducts, while in contrast, TCQN is sandwiched between two pairs of Au(I) CTCs giving 2:1 adducts without any coordination of its cyanide groups to Au(I) metal centers. Gold(I) CTCs could even form supramolecular assemblies upon acid−base interaction with CTCs of other metals, e.g., Hg(II).[13d] DFT calculations reveal that the supramolecular infite chains formed are stabilized by electrostatic interactions between the Hg_3 and the Au_3 metallic rings. The supramolecular stacks formed by $\{[3,5$-$(CF_3)_2Pz]Au\}_3$ (Pz = pyrazolate) CTCs were found[13e] to exhibit remarkable luminescence properties. Toluene

molecules intercalate between the $\{[3,5$-$(CF_3)_2Pz]Au\}_3$ CTCs, yielding the $\{[Au_3]_2$:toluene$\}_\infty$ infinite chains, and this is the first acid−base adduct ever reported in which a Au(I) CTC acts as an acid. The electronic structure and spectroscopic properties of $\{Au_3(CH_3N{=}COCH_3)_3\}_n\cdot\{2,4,7$-trinitro-9-fluorenone$\}$ (n = 1, 2) stacks were also studied theoretically employing HF, MP2, and DFT methods.[14]

On the other hand, the coinage metal halides *c*-$M_3(\mu_2$-X$)_3$ (M = Cu, Ag, or Au; X = F, Cl, Br, or I) are of importance due to their relevance with photography, printing and reprographic domain, X-ray photography in medicine and materials, and documentation.[15] In contrast to most of the metal halides, the high-temperature vapors of the coinage metal halides consist mainly of *c*-$M_3(\mu_2$-X$)_3$ (M = Cu or Ag) CTCs.[16] A rather significant number of experimental and theoretical studies have been devoted to study the Cu(I) and Ag(I) halide CTCs.[16,17] In contrast, to the best of our knowledge, studies of the respective Au(I) halide CTCs are rather scarce. Very recently, Rabilloud employing DFT methods investigated the *c*-$Au_3(\mu_2$-X$)_3$ (X = F, Cl)[18] and *c*-$Au_3(\mu_2$-X$)_3$ (X = Br, I)[19] CTCs and found that Au_3Br_3 and Au_3I_3 CTCs are particularly stable due to the onset of Au−X ion−covalent interactions with a strong covalent component. Rabilloud concluded also that in all Au(I) halide CTCs, Au−Au interactions further strengthen the cyclic trimeric aggregation of the Au atoms.

The work presented herein addresses the following issues concerning the aromatic interactions between the *c*-$Au_3(\mu_2$-X$)_3$ CTCs and the benzene, hexafluorbenzene, and borazine aromatics: (i) To compute the molecular and electronic structures, stabilities, bonding features, and magnetotropicity of the columnar binary stacks with general formula $[c$-$Au_3(\mu_2$-X$)_3]_n(L)_m$ (X = halide; L = C_6H_6, C_6F_6, or $B_3N_3H_6$; n, $m \leq 2$) we employed electronic structure calculation methods. (ii) To shed some light on the nature of the aromatic interactions in these binary stacks and estimate the impact of aromaticity we selected three diverse aromatics exhibiting different diatropic ring currents, electric molecular quadrupole moments, and polarizabilities. (iii) To analyze exhaustively the aromatic interactions in the $[c$-$Au_3(\mu_2$-X$)_3]\cdots(L)$ binary stacks, the *c*-$Au_3(\mu_2$-X$)_3$ CTCs and their $[c$-$Au_3(\mu_2$-X$)_3]_n(L)_m$ binary stacks could be considered as building blocks of gold monolayer sheets and bulk systems of aromatic molecules adsorbed on metallic surfaces. Accordingly, to fully understand the nature of the aromatic interactions in the $[c$-$Au_3(\mu_2$-X$)_3]\cdots(L)$ binary stacks we applied a multitude of theoretical techniques such as charge and energy decomposition analysis (CDA and EDA), NBO population analysis, as well as molecular electrostatic potential (MEP) calculations. These theoretical techniques were also employed to further delineate the nature of the M−X bond in gold(I) halide CTCs. (iv) To understand the through-space electron delocalization between the stacked molecules by exploitation of the effect of the $[c$-$Au_3(\mu_2$-X$)_3]\cdots(L)$ stacking on the magnetotropicity of both the *c*-$Au_3(\mu_2$-X$)_3$ and L constituents for this phenomenon is of potential interest in the field of molecular electronics. (v) To search for possible relationships between the interaction energy and its components (electrostatic, covalent, dispersion, and Pauli energy terms) and calculated physical properties.

2. COMPUTATIONAL DETAILS

Full geometry optimization without symmetry constraints was carried out for the *c*-$Au_3(\mu_2$-X$)_3$ and $[c$-$Au_3(\mu_2$-X$)_3]_n(L)_m$ species employing Truhlar's M05-2X hybrid functional,[20] which is among the best single-reference method for noncovalent complexes combined with
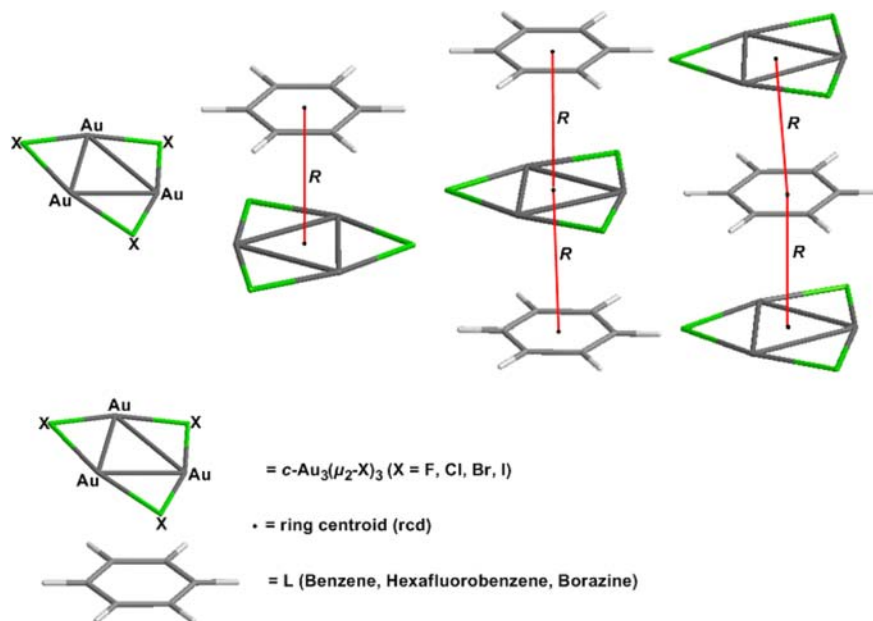
Scheme 1

compound	R (Å)	compound	R (Å)	compound	R (Å)
$[c\text{-}Au_3(\mu_2\text{-}F)_3](C_6H_6)$	3.077	$[c\text{-}Au_3F_2(\mu_2\text{-}F)(\eta^3\text{-}C_6H_6)_2]$	2.392	$[c\text{-}Au_3(\mu_2\text{-}F)_3]_2(C_6H_6)$	3.098
$[c\text{-}Au_3(\mu_2\text{-}F)_3](C_6F_6)$	3.208	$[c\text{-}Au_3(\mu_2\text{-}F)_3](C_6F_6)_2$	3.201	$[c\text{-}Au_3(\mu_2\text{-}F)_3]_2(C_6F_6)$	3.295
$[c\text{-}Au_3(\mu_2\text{-}F)_3](B_3N_3H_6)$	3.060	$[c\text{-}Au_3(\mu_2\text{-}F)_3](B_3N_3H_6)_2$	3.061	$[c\text{-}Au_3(\mu_2\text{-}F)_3]_2(B_3N_3H_6)$	3.066
$[c\text{-}Au_3(\mu_2\text{-}Cl)_3](C_6H_6)$	3.280	$[c\text{-}Au_3(\mu_2\text{-}Cl)_3](C_6H_6)_2$	3.321	$[c\text{-}Au_3(\mu_2\text{-}Cl)_3]_2(C_6H_6)$	3.292
$[c\text{-}Au_3(\mu_2\text{-}Cl)_3](C_6F_6)$	3.341	$[c\text{-}Au_3(\mu_2\text{-}Cl)_3](C_6F_6)_2$	3.338	$[c\text{-}Au_3(\mu_2\text{-}Cl)_3]_2(C_6F_6)$	3.341
$[c\text{-}Au_3(\mu_2\text{-}Cl)_3](B_3N_3H_6)$	3.292	$[c\text{-}Au_3(\mu_2\text{-}Cl)_3](B_3N_3H_6)_2$	3.334	$[c\text{-}Au_3(\mu_2\text{-}Cl)_3]_2(B_3N_3H_6)$	3.304
$[c\text{-}Au_3(\mu_2\text{-}Br)_3](C_6H_6)$	3.322	$[c\text{-}Au_3(\mu_2\text{-}Br)_3](C_6H_6)_2$	3.375	$[c\text{-}Au_3(\mu_2\text{-}Br)_3]_2(C_6H_6)$	3.335
$[c\text{-}Au_3(\mu_2\text{-}Br)_3](C_6F_6)$	3.378	$[c\text{-}Au_3(\mu_2\text{-}Br)_3](C_6F_6)_2$	3.381	$[c\text{-}Au_3(\mu_2\text{-}Br)_3]_2(C_6F_6)$	3.379
$[c\text{-}Au_3(\mu_2\text{-}Br)_3](B_3N_3H_6)$	3.334	$[c\text{-}Au_3(\mu_2\text{-}Br)_3](B_3N_3H_6)_2$	3.498	$[c\text{-}Au_3(\mu_2\text{-}Br)_3]_2(B_3N_3H_6)$	3.460
$[c\text{-}Au_3(\mu_2\text{-}I)_3](C_6H_6)$	3.394	$[c\text{-}Au_3(\mu_2\text{-}I)_3](C_6H_6)_2$	3.476	$[c\text{-}Au_3(\mu_2\text{-}I)_3]_2(C_6H_6)$	3.407
$[c\text{-}Au_3(\mu_2\text{-}I)_3](C_6F_6)$	3.450	$[c\text{-}Au_3(\mu_2\text{-}I)_3](C_6F_6)_2$	3.452	$[c\text{-}Au_3(\mu_2\text{-}I)_3]_2(C_6F_6)$	3.448
$[c\text{-}Au_3(\mu_2\text{-}I)_3](B_3N_3H_6)$	3.414	$[c\text{-}Au_3(\mu_2\text{-}I)_3](B_3N_3H_6)_2$	3.610	$[c\text{-}Au_3(\mu_2\text{-}I)_3]_2(B_3N_3H_6)$	3.545

the Def2-TZVPP basis set[21] for all atoms (the computational approach is denoted as M05-2X/Def2-TZVPP). All optimization and binding energy calculations were performed using the Gaussian09 suite of programs[22] employing an ultrafine integration grid specified as Int(Grid = −96032). Attainment of the energy minimum was verified by calculating the harmonic vibrational frequencies that result in the absence of imaginary eigenvalues (NImag = 0). Computed electronic energies were corrected to constant pressure and 298 K for zero-point energy (ZPE) differences and the contributions of the translational, rotational, and vibrational partition functions. Basis set superposition error (BSSE) was calculated using the counterpoise method[23,24] as implemented in the Gaussian09 software.[22] It should be noted that whatever the initial orientation of the starting geometry, calculations were always converged to the columnar binary stack with parallel orientation. The natural bond orbital (NBO) population analysis was performed using Weinhold's methodology.[25] Magnetic shielding tensors have been computed with the GIAO (gauge-including atomic orbitals) DFT method[26] as implemented in the Gaussian09 series of programs[22] employing the B3LYP hybrid functional[27] in combination with the Def2-TZVPP basis set (denoted as GIAO/B3LYP/Def2-TZVPP). Nucleus-independent chemical shift (NICS) values were computed at the same level according to the procedure described by Schleyer et al.[28] The magnetic shielding tensor element was calculated for a ghost atom, Bq, located at the center of the ring. Negative (diatropic) NICS values indicate aromaticity, while positive (para-

tropic) values imply antiaromaticity. Charge decomposition analysis (CDA) developed by Frenking et al.[29] was performed as implemented in the latest version of the AOMix software[30] using the M05-2X/Def2-TZVPP method. Energy decomposition analysis (EDA) calculations[31] were performed as implemented in the ADF 2010.01 program package.[32] EDA calculations were performed at the revPBE-D3/TZ2P level of theory, while scalar relativistic effects have been considered using the zero-order regular approximation (ZORA).[33] The revPBE-D3 is a meta GGA functional which includes dispersion corrections.[34] The TZ2P basis set is of triple-ζ quality augmented with one set of polarization functions, i.e., p functions on hydrogen, d functions on carbon, and f functions for the transition metal atoms, while the core electrons of all atoms are treated with the frozen core approximation.[35] The RDG (reduced density gradient) plots were obtained employing the Multiwfn software version 2.2.1.[36]

3. RESULTS AND DISCUSSION

3.1. Structural, Electronic, and Bonding Properties of the $[c\text{-}Au_3(\mu_2\text{-}X)_3]_n(L)_m$ (X = Halide; L = C_6H_6, C_6F_6, or $B_3N_3H_6$; n, $m \leq 2$) Binary Stacks. The schematic representation of the equilibrium geometries of the $[c\text{-}Au_3(\mu_2\text{-}X)_3]_n(L)_m$ (X = halide; L = C_6H_6, C_6F_6, or $B_3N_3H_6$; n, $m \leq 2$) binary stacks and the $c\text{-}Au_3(\mu_2\text{-}X)_3$ CTCs are shown in Scheme 1. Selected structural parameters of the $[c\text{-}Au_3(\mu_2\text{-}X)_3]_n(L)_m$ (X = halide; L = C_6H_6,

C_6F_6, or $B_3N_3H_6$; n, $m \leq 2$) binary stacks and the c-$Au_3(\mu_2$-$X)_3$ CTCs computed at the M05-2X/Def2-TZVPP level are given in the Supporting Information (Figures S1−S3). The optimized intermolecular distances, R, between the ring centroids (rcd) of the stacking participants calculated at the M05-2X/Def2-TZVPP level are collected in Table 1.

The c-$Au_3(\mu_2$-$X)_3$ clusters are planar molecules with D_{3h} symmetry, except c-$Au_3(\mu_2$-$Cl)_3$ which has C_{3h} symmetry. The significant deviation of the structure of these molecules from the perfect hexagonal arrangement of the gold and halide atoms, corresponding to D_{6h} symmetry, indicates that they are not pure ionic systems. Earlier experimental and theoretical studies concluded that this holds also true for the rest of the coinage metal halide CTCs, namely, c-$Cu_3(\mu_2$-$X)_3$ and c-$Ag_3(\mu_2$-$X)_3$.[16,17,37] The bridging halide ligands form perfect isosceles triangles with the bridged gold(I) atoms comprising the triangular metallic ring.

Generally, formation of the $[c$-$Au_3(\mu_2$-$X)_3]_n(L)_m$ (X = halide; L = C_6H_6, C_6F_6, or $B_3N_3H_6$; n, $m \leq 2$) binary stacks is accompanied by small and even marginal structural changes. In particular, a small "shrinkage" and/or "enlargement" of the Au_3 ring in the $[c$-$Au_3(\mu_2$-$X)_3]_n(L)_m$ **pff** stacks relative to the size of the Au_3 ring in the corresponding "free-standing" c-$Au_3(\mu_2$-$X)_3$ CTCs is observed as a result of the diverse aromatic interactions characterizing the $[c$-$Au_3(\mu_2$-$X)_3]_n(L)_m$ **pff** stacks due to the diverse physical properties of the aromatic L (L = C_6H_6, C_6F_6, $B_3N_3H_6$) stacking participants, which are important determinants of the aromatic interactions (consisting of covalent, electrostatic, and dispersion forces). These properties for the C_6H_6, C_6F_6, and $B_3N_3H_6$ ligands and the "free-standing" c-$Au_3(\mu_2$-$X)_3$ CTCs are tabulated in Table 2.

Table 2. zz Tensor Components of Quadrupole Moments, Q_{zz}, Polarizabilities, α_{zz}, and Nucleus-Independent Chemical Shift, $NICS_{zz}(1)$, along with the Molecular Electrostatic Potential, MEP(0), and Surface Area of C_6H_6, C_6F_6, $B_3N_3H_6$, and c-$Au_3(\mu_2$-$X)_3$ Clusters

compound	Q_{zz} (D-Å)	α_{zz} (au)	MEP(0) (au)	$NICS_{zz}(1)$ (ppm)	surface area (Å²)
C_6H_6	-28.3 ± 1.2^a	76.3	0.27	-30.1	31.6
C_6F_6	$+34.0^a$	80.2	0.13	-23.2	38.1
$B_3N_3H_6$	-10.6 ± 1.3^b	41.3	0.12	-6.3	33.2
c-$Au_3(\mu_2$-$F)_3$	-86.0	78.7	0.14	2.2	20.3
c-$Au_3(\mu_2$-$Cl)_3$	-106.4	137.6	0.12	8.3	24.5
c-$Au_3(\mu_2$-$Br)_3$	-124.4	165.7	0.10	10.5	26.2
c-$Au_3(\mu_2$-$I)_3$	-147.0	215.9	0.08	13.5	28.7

^{a}Experimental values taken from ref 38. ^{b}Experimental values taken from ref 39.

It is worth noticing that Q_{zz} is related to the electrostatic and dispersion forces, MEP(0) is related to the electrostatic forces, α_{zz} is related to covalent and dispersion forces, while $NICS_{zz}(1)$ is related to the induced magnetic fields B_z^{ind} at 1 Å above the ring planes of the C_6H_6, C_6F_6, and $B_3N_3H_6$ ligands and the c-$Au_3(\mu_2$-$X)_3$ CTCs and therefore could account for the coupling of the induced magnetic fields of the superimposed stacking participants.

All 1:1 $[c$-$Au_3(\mu_2$-$X)_3](L)$ (L = C_6H_6, C_6F_6, $B_3N_3H_6$) binary stacks adopt the **pff** conformation. In the 1:2 $[c$-$Au_3(\mu_2$-$X)_3](L)_2$ binary stacks the c-$Au_3(\mu_2$-$X)_3$ moieties retaining their

planar structure are also in almost perfect parallel face-to-face, **pff**, orientation, with the two benzene, hexafluorobenzene, and borazine stacking participants, except the $[c$-$Au_3(\mu_2$-$X)_3]$-$(B_3N_3H_6)_2$ (X = Br, I) binary stacks which adopt the offset face-to-face, **osff**, conformation and the $[c$-$Au_3(\mu_2$-$F)_3](C_6H_6)_2$ binary stack where the ring planes of the benzene stacking participants are not parallel to the Au_3 ring plane; the centroids of the rings form an angle of 134.2° (Figure S2, Supporting Information). In the $[c$-$Au_3(\mu_2$-$Br)_3](B_3N_3H_6)_2$ and $[c$-$Au_3(\mu_2$-$I)_3]$ $(B_3N_3H_6)_2$ **osff** stacks the ring centroids of the stacking participants form angles of 169.2° and 167.3°, respectively. In the $[c$-$Au_3(\mu_2$-$F)_3](C_6H_6)_2$ binary stack and the $[c$-$Au_3(\mu_2$-$X)_3]$ $(B_3N_3H_6)_2$ (X = Br, I) **osff** stacks the c-$Au_3(\mu_2$-$X)_3$ CTCs adopt C_{2v} symmetry with the Au_3 triangle becoming an isosceles triangle. The c-$Au_3(\mu_2$-$X)_3$ CTCs in the 2:1 $[c$-$Au_3(\mu_2$-$X)_3]_2(L)$ binary stacks also retain their planarity and are in almost perfect parallel face-to-face, **pff**, orientation with the "sandwiched" benzene, hexafluorobenzene, and borazine stacking participants, except the $[c$-$Au_3(\mu_2$-$X)_3](B_3N_3H_6)_2$ (X = Br, I) binary stacks which adopt the offset face-to-face, **osff**, conformation with the centroids of the rings forming angles of 156.2° and 151.0° for the bromo and iodo stacks, respectively (Figure S3, Supporting Information). It is worth noting that in the $[c$-$Au_3(\mu_2$-$X)_3]_2(B_3N_3H_6)$ (X = Br, I) **osff** stacks the c-$Au_3(\mu_2$-$X)_3$ stacking participants adopt C_{2v} symmetry for the Au_3 triangle becomes isosceles.

The intermolecular distance, R, between the ring centroids of the stacking participants (Scheme 1) found in the ranges 3.060−3.450, 2.932−3.610, and 3.066−3.545 Å for the 1:1, 1:2, and 2:1 binary stacks, respectively, are indicative of the existence of intermolecular interactions between the c-$Au_3(\mu_2$-$X)_3$ CTCs and the C_6H_6, C_6F_6, and $B_3N_3H_6$ stacking participants. For the $[c$-$Au_3(\mu_2$-$X)_3](L)_2$ (X = Cl, Br, I; L = C_6H_6, $B_3N_3H_6$) binary stacks the R distances are longer relative to the R distances in the corresponding 1:1 binary stacks but comparable to the R distances of the corresponding 2:1 $[c$-$Au_3(\mu_2$-$X)_3]_2(L)$ binary stacks. Noteworthy, in the $[c$-$Au_3(\mu_2$-$F)_3](C_6H_6)_2$ binary stack which adopts the peculiar structure with the benzene rings inclined with respect to the Au_3 ring the R distance is shorter (by 0.145 Å) relative to the R distance of the 1:1 $[c$-$Au_3(\mu_2$-$F)_3](C_6H_6)$ **pff** stack. Furthermore, in the $[c$-$Au_3(\mu_2$-$F)_3](C_6H_6)_2$ binary stack the central c-Au_3F_3 stacking participant is dramatically affected by the stacking interactions and converted to a triangular structure (isosceles triangle) having one bridging and two terminal fluoride ligands, thus formulated as c-$Au_3F_2(\mu_2$-$F)$. In addition, the benzene stacking participants in the $[c$-$Au_3(\mu_2$-$F)_3](C_6H_6)_2$ compound also undergo significant structural changes, with the C−C bonds becoming unequivalent. This effect could be explained by taking into account the stronger interactions of the benzene molecules with one of the Au atoms and are also responsible for rupture of the Au−F bonds of the particular Au atom (the estimated Au···F distances are found to be 3.199 Å), rendering the fluoride ligands terminal.

The estimated R distances in the $[c$-$Au_3(\mu_2$-$X)_3]_n(L)_m$ (X = halide; L = C_6H_6, C_6F_6, or $B_3N_3H_6$; n, $m \leq 2$) binary stacks increase along the series of the fluoro, chloro, bromo, and iodo stacks for all three C_6H_6, C_6F_6, and $B_3N_3H_6$ stacking participants. Moreover, we found that the estimated R distances are linearly correlated with Q_{zz}, MEP(0), α_{zz}, and $NICS_{zz}$, as it is clearly shown in Figure 1. These linear relationships are indicative of the contribution of electrostatic, dispersion, and charge transfer interactions to the stacking interactions intrinsic
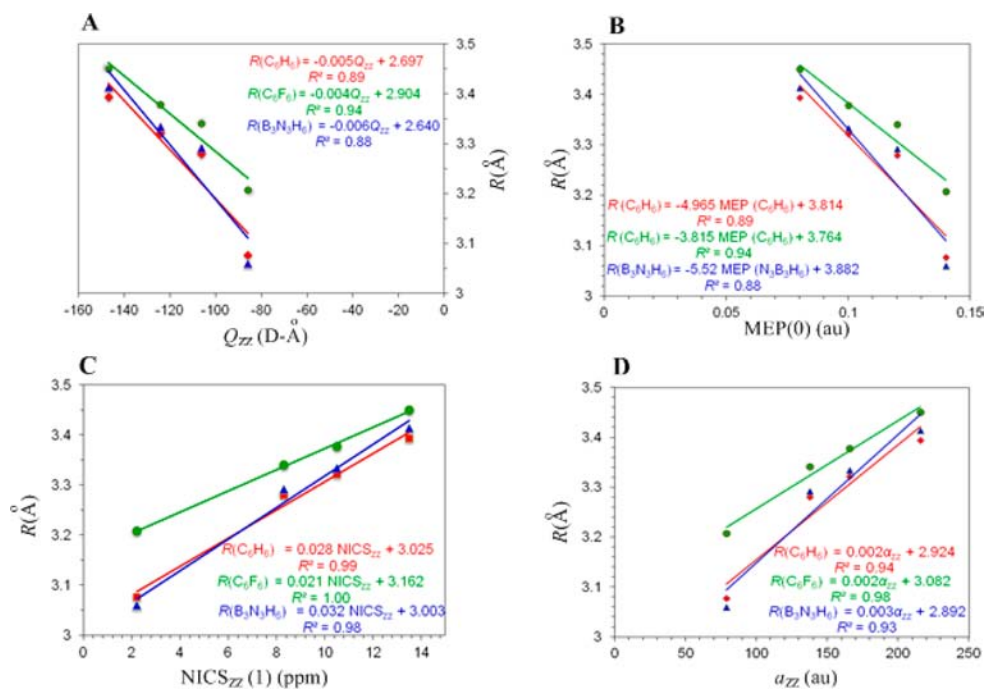
Figure 1. Linear correlations of the intermolecular distance of the $[c\text{-}Au_3(\mu_2\text{-}X)_3](L)$ **pff** stacks with the zz tensor component of quadrupole moment, Q_{zz} (A), the molecular electrostatic potential, MEP(0) (B), the zz tensor component of the nucleus-independent chemical shift, $NICS_{zz}(1)$ (1 Å above the corresponding ring center) (C), and the polarizability α_{zz} (D) of the $c\text{-}Au_3(\mu_2\text{-}X)_3$ CTCs computed at the M05-2X/Def2-TZVPP level.

to $[c\text{-}Au_3(\mu_2\text{-}X)_3]_n(L)_m$ (X = halide; L = C_6H_6, C_6F_6, or $B_3N_3H_6$; n, $m \leq 2$) binary stacks.

In order to get insight into the interplay of electrostatics, charge transfer, and dispersion in the $[c\text{-}Au_3(\mu_2\text{-}X)_3]_n(L)_m$ (X = halide; L = C_6H_6, C_6F_6, or $B_3N_3H_6$; n, $m \leq 2$) **pff** binary stacks we investigated them further by employing energy decomposition analysis (EDA) and charge decomposition analysis (CDA) based on revPBE-D3/TZ2P and M05-2X/Def2-TZVPP calculations, respectively. EDA and CDA results are compiled in Tables 3 and 4, respectively. Notice that the interaction energies, ΔE_{int}, were calculated considering the $[c\text{-}Au_3(\mu_2\text{-}X)_3](L) \rightarrow [c\text{-}Au_3(\mu_2\text{-}X)_3] + L$, $[c\text{-}Au_3(\mu_2\text{-}X)_3](L)_2 \rightarrow [c\text{-}Au_3(\mu_2\text{-}X)_3](L) + L$, and $[c\text{-}Au_3(\mu_2\text{-}X)_3]_2(L) \rightarrow [c\text{-}Au_3(\mu_2\text{-}X)_3](L) + [c\text{-}Au_3(\mu_2\text{-}X)_3]$ dissociation processes.

Inspection of Table 3 reveals that the orbital interactions term, ΔE_{orb}, is estimated to be relatively small while the dominant contributions to the interaction energy ΔE_{int} arise from the electrostatic (ΔE_{elstat}) and dispersion (ΔE_{disp}) energy terms. In the $[c\text{-}Au_3(\mu_2\text{-}X)_3](L)$ **pff** stacks, except $[c\text{-}Au_3(\mu_2\text{-}F)_3](C_6H_6)]$ and $[c\text{-}Au_3(\mu_2\text{-}F)_3](B_3N_3H_6)$, ΔE_{disp} has a much higher contribution to ΔE_{int} than ΔE_{elstat}, while in $[c\text{-}Au_3(\mu_2\text{-}F)_3](C_6H_6)$, ΔE_{elstat} overwhelms ΔE_{disp}, and in $[c\text{-}Au_3(\mu_2\text{-}F)_3](B_3N_3H_6)$ ΔE_{disp} and ΔE_{elstat} contribute almost equally to ΔE_{int}.

In the 1:2 $[c\text{-}Au_3(\mu_2\text{-}X)_3](L)_2$ (X = F, Cl, Br, I; L = C_6H_6, C_6F_6, $B_3N_3H_6$) **pff** stacks, except $[c\text{-}Au_3(\mu_2\text{-}F)_3](C_6H_6)_2$ and $[c\text{-}Au_3(\mu_2\text{-}F)_3](B_3N_3H_6)_2$, the dominant contributions to ΔE_{int} arise from the dispersion energy term, ΔE_{disp} (50−67%). The contribution of the ΔE_{disp} energy terms to ΔE_{int} follows the trend I > Br > Cl > F. For the peculiar structure of $[c\text{-}Au_3(\mu_2\text{-}F)_3](C_6H_6)_2$ binary stack the EDA results illustrate the strong contribution of ΔE_{elstat} (54%) and ΔE_{orb} (35%) energy terms to the interaction energy ΔE_{int} while ΔE_{disp} contributes less (11%). The strong covalent interactions featuring the bonding of the two benzene stacking participants to one of the Au atoms

of the triangular Au_3 ring in a η^3-coordination mode in the $[c\text{-}Au_3(\mu_2\text{-}F)_3](C_6H_6)_2$ binary stack are supported by in-phase orbital interactions; their 3D plots are shown in Scheme 2.

In the 2:1 $[c\text{-}Au_3(\mu_2\text{-}X)_3]_2(L)$ (X = F, Cl, Br, I; L = C_6H_6, C_6F_6, $B_3N_3H_6$) "sandwiches", except $[c\text{-}Au_3(\mu_2\text{-}F)_3]_2(C_6H_6)$, the interactions are also dominated by the dispersion forces; the ΔE_{disp} energy terms contribute 40−59% to the interaction energy ΔE_{int}. In the $[c\text{-}Au_3(\mu_2\text{-}F)_3]_2(C_6H_6)$ stack ΔE_{disp} and ΔE_{elstat} contribute almost equally, e.g., 37% and 41%, respectively, to ΔE_{int}. For the benzene, hexafluorobenzene, and borazine "sandwiches" ΔE_{disp} contributes to ΔE_{int} 50−56%, 49−59%, and 40−55%, while the contribution of ΔE_{elstat} amounts to 30−34%, 28−31%, and 28−35%, respectively. Noteworthy, the contribution of ΔE_{orb} to ΔE_{int} is also significant (13−25%), particularly in the $[c\text{-}Au_3(\mu_2\text{-}F)_3]_2(L)$ (L = C_6H_6, C_6F_6, $B_3N_3H_6$) "sandwiches". As in the case of the 1:2 binary stacks, the contribution of ΔE_{disp} to ΔE_{int} of the 2:1 binary stacks follows the trend I > Br > Cl > F.

The interaction energies ΔE_{int} of the $[c\text{-}Au_3(\mu_2\text{-}X)_3]_n(L)_m$ (X = halide; L = C_6H_6, C_6F_6, or $B_3N_3H_6$; n, $m \leq 2$) **pff** binary stacks calculated at the revPBE-3D/TZ2P level found to be in the range from −9.4 to −15.6 kcal/mol are comparable to the calculated ΔE_{int} values for the $[c\text{-}M_3(\mu_2\text{-}X)_3](C_6H_6)$ (M = Cu or Ag) binary stacks.[6] From analysis of the interaction energy ΔE_{int} of the $[c\text{-}Au_3(\mu_2\text{-}X)_3]_n(L)_m$ (X = halide; L = C_6H_6, C_6F_6, or $B_3N_3H_6$; n, $m \leq 2$) **pff** stacks it becomes evident that electrostatic and dispersion forces dominate the interactions between $c\text{-}Au_3(\mu_2\text{-}X)_3$ and L with a small contribution of covalent interactions (ΔE_{orb}). This conclusion is further corroborated by testing for general correlations of ΔE_{int} and its components (ΔE_{disp}, ΔE_{elstat}, ΔE_{orb}, and ΔE_{Pauli}) with calculated physical properties related to dispersion and electrostatic forces. The linear relationships obtained are given in the Supporting Information (Table S1 and Figures S4−S5).

Table 3. Energy Decomposition Analysis (EDA) of the Aromatic Interactions in the $[c\text{-Au}_3(\mu_2\text{-X})_3]_n(L)_m$ (X = halide; L = C_6H_6, C_6F_6, or $B_3N_3H_6$; n, $m \leq 2$) pff Binary Stacks Computed at the revPBE-D3/TZ2P Level^a

compound	ΔE_{int}	ΔE_{Pauli}	ΔE_{elstat}	ΔE_{orb}	ΔE_{disp}	compound	ΔE_{int}	ΔE_{Pauli}	ΔE_{elstat}	ΔE_{orb}	ΔE_{disp}
$[c\text{-Au}_3(\mu_2\text{-F})_3](C_6H_6)$	−11.28	36.37	−21.07	−10.50	−16.38	$[c\text{-Au}_3(\mu_2\text{-Br})_3](C_6F_6)$	−12.00	20.87	−9.59	−4.78	−18.50
$[c\text{-Au}_3F_2(\mu_2\text{-F})(\eta^3\text{-}C_6H_6)_2]$	−27.63	109.84	−73.36	−48.52	−15.59	$[c\text{-Au}_3(\mu_2\text{-Br})_3](C_6F_6)_2$	−12.12	20.73	−9.45	−4.67	−18.73
$[c\text{-Au}_3(\mu_2\text{-F})_3]_2(C_6H_6)$	−11.68	34.28	−18.85	−10.04	−17.07	$[c\text{-Au}_3(\mu_2\text{-Br})_3]_2(C_6F_6)$	−13.02	20.84	−9.53	−4.85	−19.49
$[c\text{-Au}_3(\mu_2\text{-Cl})_3](C_6H_6)$	−11.22	25.30	−13.18	−6.05	−17.28	$[c\text{-Au}_3(\mu_2\text{-I})_3](C_6F_6)$	−12.34	20.27	−9.40	−4.44	−18.78
$[c\text{-Au}_3(\mu_2\text{-Cl})_3](C_6H_6)_2$	−10.95	23.50	−12.21	−4.99	−17.26	$[c\text{-Au}_3(\mu_2\text{-I})_3](C_6F_6)_2$	−12.42	20.48	−9.45	−4.37	−19.08
$[c\text{-Au}_3(\mu_2\text{-Cl})_3]_2(C_6H_6)$	−11.98	24.43	−12.45	−5.89	−18.08	$[c\text{-Au}_3(\mu_2\text{-I})_3]_2(C_6F_6)$	−13.45	20.45	−9.38	−4.47	−20.05
$[c\text{-Au}_3(\mu_2\text{-Br})_3](C_6H_6)$	−11.46	24.13	−12.43	−5.42	−17.75	$[c\text{-Au}_3(\mu_2\text{-F})_3](B_3N_3H_6)$	−14.95	34.06	−18.23	−11.86	−18.91
$[c\text{-Au}_3(\mu_2\text{-Br})_3](C_6H_6)_2$	−11.22	22.18	−11.38	−4.39	−17.63	$[c\text{-Au}_3(\mu_2\text{-F})_3](B_3N_3H_6)_2$	−15.19	34.18	−18.51	−11.58	−19.28
$[c\text{-Au}_3(\mu_2\text{-Br})_3]_2(C_6H_6)$	−12.49	23.38	−11.90	−5.32	−18.65	$[c\text{-Au}_3(\mu_2\text{-F})_3]_2(B_3N_3H_6)$	−15.64	33.23	−17.22	−11.95	−19.69
$[c\text{-Au}_3(\mu_2\text{-I})_3](C_6H_6)$	−11.19	22.38	−10.58	−5.03	−17.96	$[c\text{-Au}_3(\mu_2\text{-Cl})_3](B_3N_3H_6)$	−12.90	22.13	−10.54	−6.01	−18.47
$[c\text{-Au}_3(\mu_2\text{-I})_3](C_6H_6)_2$	−10.84	19.75	−9.23	−3.91	−17.46	$[c\text{-Au}_3(\mu_2\text{-Cl})_3](B_3N_3H_6)_2$	−12.74	21.02	−10.06	−5.29	−18.41
$[c\text{-Au}_3(\mu_2\text{-I})_3]_2(C_6H_6)$	−12.47	21.80	−10.24	−4.96	−19.07	$[c\text{-Au}_3(\mu_2\text{-Cl})_3]_2(B_3N_3H_6)$	−13.77	21.30	−9.97	−5.97	−19.13
$[c\text{-Au}_3(\mu_2\text{-F})_3](C_6F_6)$	−9.42	24.26	−10.88	−6.42	−16.38	$[c\text{-Au}_3(\mu_2\text{-Br})_3](B_3N_3H_6)$	−12.82	21.30	−9.99	−5.38	−18.74
$[c\text{-Au}_3(\mu_2\text{-F})_3](C_6F_6)_2$	−9.62	24.46	−11.01	−6.37	−16.69	$[c\text{-Au}_3(\mu_2\text{-Br})_3](B_3N_3H_6)_2$	−12.54	22.15	−11.06	−5.12	−18.52
$[c\text{-Au}_3(\mu_2\text{-F})_3]_2(C_6F_6)$	−10.15	24.44	−10.85	−6.71	−17.03	$[c\text{-Au}_3(\mu_2\text{-Br})_3]_2(B_3N_3H_6)$	−14.01	23.11	−11.51	−5.94	−19.67
$[c\text{-Au}_3(\mu_2\text{-Cl})_3](C_6F_6)$	−11.17	20.86	−9.26	−4.88	−17.89	$[c\text{-Au}_3(\mu_2\text{-I})_3](B_3N_3H_6)$	−12.15	19.67	−8.56	−4.75	−18.51
$[c\text{-Au}_3(\mu_2\text{-Cl})_3](C_6F_6)_2$	−11.26	20.88	−9.24	−4.76	−18.15	$[c\text{-Au}_3(\mu_2\text{-I})_3](B_3N_3H_6)_2$	−12.13	21.41	−10.14	−4.86	−18.53
$[c\text{-Au}_3(\mu_2\text{-Cl})_3]_2(C_6F_6)$	−12.05	20.90	−9.27	−4.98	−18.71	$[c\text{-Au}_3(\mu_2\text{-I})_3]_2(B_3N_3H_6)$	−14.14	23.08	−11.01	−5.88	−20.34

$^a\Delta E_{int}$ values were calculated for the $[c\text{-Au}_3(\mu_2\text{-X})_3](L) \rightarrow [c\text{-Au}_3(\mu_2\text{-X})_3] + L$, $[c\text{-Au}_3(\mu_2\text{-X})_3](L)_2 \rightarrow [c\text{-Au}_3(\mu_2\text{-X})_3](L) + L$, and $[c\text{-Au}_3(\mu_2\text{-X})_3]_2(L) \rightarrow [c\text{-Au}_3(\mu_2\text{-X})_3](L) + [c\text{-Au}_3(\mu_2\text{-X})_3]$ dissociation processes.

Generally, ΔE_{int} correlates very well with the zz tensor component of the quadrupole moment, Q_{zz} (cf. Table S1, Supporting Information), for all pff binary stacks. This is expected for the quadrupolar effect accounts for the permanent polar and electrostatic effects, which are important effects in aromatic pff stacks.[40] The zz tensor component of the polarizability, α_{zz}, correlates also very well with ΔE_{int}, ΔE_{elstat}, ΔE_{orb}, and ΔE_{Pauli} (cf. Table S1, Supporting Information), except the worst correlations α_{zz} vs ΔE_{elstat} for the C_6F_6 ($R^2 = 0.61$) and α_{zz} vs ΔE_{disp} for the borazine ($R^2 = 0.46$) pff stacks, respectively. Excellent linear correlations were obtained between α_{zz} and ΔE_{orb} and ΔE_{Pauli}. Interestingly, the best correlations ($R^2 = 0.90-0.98$) were obtained between the $NICS_{zz}(1)$ magnetic criterion of aromaticity and ΔE_{int}, indicating significant contribution arising from charge transfer between the stacking participants. Good linear relationships ($R^2 = 0.87-0.96$) were also obtained for the correlations between the surface area, S, and ΔE_{int} and all of its components (ΔE_{elstat}, ΔE_{disp}, ΔE_{orb}, and ΔE_{Pauli}), except again for the worst correlations S vs ΔE_{elstat} for the C_6F_6 ($R^2 = 0.69$) and S vs ΔE_{disp} for the borazine ($R^2 = 0.50$) pff stacks. Noteworthy, S seems to be an important factor in stacking interactions. The different flavor of the aromatic interactions in the hexafluorobenze than in the benzene and borazine pff stacks could be accounted for by the different electrostatic potentials of hexafluorobenze, benzene, and borazine molecules in relation with the electrostatic potentials of the $c\text{-Au}_3(\mu_2\text{-X})_3$ CTCs shown in Figure 2.

Perusal of Figure 2 reveals that in all $c\text{-Au}_3(\mu_2\text{-X})_3$ CTCs there is a positive region delocalized over the entire triangular metallic ring core, while negative regions are located on the bridging halide ligands. On the other hand, in the benzene and borazine molecules there is a negative region delocalized over the center of the six-membered rings and positive regions are located on the peripheral hydrogen atoms, whereas in hexafluorobenzene there is a positive region delocalized over the entire ring plane. From the simple electrostatic picture, one could deduce that the pff stacks should be most favorable for the benzene and borazine stacks and the offset face-to-face (osff) stacks for the hexafluorobenzene stacks in order to avoid the Coulomb repulsion of two areas with similar MEP. However, the C_6F_6 stacks with the $c\text{-Au}_3(\mu_2\text{-X})_3$ CTCs prefer also the pff orientation, indicating the pitfalls of using the simple electrostatic picture for understanding stacking interactions.[41] Cundari et al.,[5] using DFT calculations of MEP, assessed the π acidity and π basicity of metallorganic trimetallic macromolecular complexes of the type $[M(\mu\text{-L})]_3$, where M = Cu, Ag, or Au and L = carbeniate, imidazolate, pyridiniate, pyrazolate, or triazolate, comparing them with various organic compounds, e.g., benzene, pyrazole, imidazole, pyridine, and triazole. Accordingly, the $c\text{-Au}_3(\mu_2\text{-X})_3$ clusters are expected to behave as π acids interacting with the π bases benzene and borazine molecules.

CDA calculations at the M05-2X/Def2-TZVPP level (Table 4) illustrated further the charge transfer from L (L = C_6H_6, C_6F_6, $B_3N_3H_6$) to $c\text{-Au}_3(\mu_2\text{-X})_3$ CTCs in the binary stacks studied. The net charge donation from L toward the $c\text{-Au}_3(\mu_2\text{-X})_3$ CTCs is estimated to be about 0.005–0.136 |e|. The negative values of the charge polarization term, r, mean that electronic charge of about 0.08–0.14 |e|, 0.09–0.23 |e|, and 0.09–0.13 |e| is be removed from the occupied/occupied region of the fragment orbitals into the nonoverlapping regions upon formation of the 1:1, 1:2, and 2:1 binary stacks (reduced closed-shell repulsion in comparison with the superimposed fragments), respectively. Finally, the very small values of the rest term, Δ, indicate that the interactions between the $c\text{-Au}_3(\mu_2\text{-X})_3$ CTCs and L in the studied binary stacks involve also donor−acceptor interactions. It is worth noting that the net charge donation from L toward the $c\text{-Au}_3(\mu_2\text{-X})_3$ CTCs correlates very well with all physical properties considered herein (Figure 3).

Noteworthy, the best correlation is the q_{NCD} vs $NICS_{zz}(1)$ ($R^2 = 0.99$), indicating once again that the $NICS_{zz}(1)$ magnetic criterion of aromaticity should probably be a good descriptor of the electron delocalization of the stacking participants in their pff binary stacks.

Table 4. Charge Decomposition Analysis (CDA) of the Aromatic Interactions in the $[c\text{-}Au_3(\mu_2\text{-}X)_3]_n(L)_m$ (X = halide; L = C_6H_6, C_6F_6, or $B_3N_3H_6$; n, $m \leq 2$) pff Binary Stacks Computed at the M05-2X/Def2-TZVPP Level

compound	$D_0{}^a$	r	Δ	$q_{NCD}{}^b$
$[c\text{-}Au_3(\mu_2\text{-}F)_3](C_6H_6)$	−10.2	−0.136	0.002	0.009
$[c\text{-}Au_3F_2(\mu_2\text{-}F)(\eta^3\text{-}C_6H_6)_2]$	−32.0	−0.227	−0.003	0.181
$[c\text{-}Au_3(\mu_2\text{-}F)_3]_2(C_6H_6)$	−8.2	−0.130	0.000	0.038
$[c\text{-}Au_3(\mu_2\text{-}Cl)_3](C_6H_6)$	−7.4	−0.121	0.001	0.026
$[c\text{-}Au_3(\mu_2\text{-}Cl)_3](C_6H_6)_2$	−6.4	−0.115	0.000	0.053
$[c\text{-}Au_3(\mu_2\text{-}Cl)_3]_2(C_6H_6)$	−6.6	−0.118	0.000	0.005
$[c\text{-}Au_3(\mu_2\text{-}Br)_3](C_6H_6)$	−7.0	−0.123	0.000	0.037
$[c\text{-}Au_3(\mu_2\text{-}Br)_3](C_6H_6)_2$	−7.8	−0.116	0.000	0.057
$[c\text{-}Au_3(\mu_2\text{-}Br)_3]_2(C_6H_6)$	−6.5	−0.121	0.000	0.019
$[c\text{-}Au_3(\mu_2\text{-}I)_3](C_6H_6)$	−6.3	−0.122	0.000	0.044
$[c\text{-}Au_3(\mu_2\text{-}I)_3](C_6H_6)_2$	−6.7	−0.111	−0.001	0.056
$[c\text{-}Au_3(\mu_2\text{-}I)_3]_2(C_6H_6)$	−5.8	−0.120	0.000	0.030
$[c\text{-}Au_3(\mu_2\text{-}F)_3](C_6F_6)$	−7.2	−0.083	−0.006	0.057
$[c\text{-}Au_3(\mu_2\text{-}F)_3](C_6F_6)_2$	−6.8	−0.087	−0.006	0.018
$[c\text{-}Au_3(\mu_2\text{-}F)_3]_2(C_6F_6)$	−4.6	−0.085	−0.007	0.068
$[c\text{-}Au_3(\mu_2\text{-}Cl)_3](C_6F_6)$	−6.4	−0.085	−0.004	0.038
$[c\text{-}Au_3(\mu_2\text{-}Cl)_3](C_6F_6)_2$	−6.8	−0.087	−0.006	0.018
$[c\text{-}Au_3(\mu_2\text{-}Cl)_3]_2(C_6F_6)$	−5.8	−0.087	−0.005	0.045
$[c\text{-}Au_3(\mu_2\text{-}Br)_3](C_6F_6)$	−7.8	−0.090	−0.004	0.026
$[c\text{-}Au_3(\mu_2\text{-}Br)_3](C_6F_6)_2$	−6.3	−0.091	−0.006	0.011
$[c\text{-}Au_3(\mu_2\text{-}Br)_3]_2(C_6F_6)$	−6.0	−0.091	−0.005	0.031
$[c\text{-}Au_3(\mu_2\text{-}I)_3](C_6F_6)$	−6.7	−0.091	−0.005	0.017
$[c\text{-}Au_3(\mu_2\text{-}I)_3](C_6F_6)_2$	−5.8	−0.093	−0.006	0.005
$[c\text{-}Au_3(\mu_2\text{-}I)_3]_2(C_6F_6)$	−6.0	−0.092	−0.005	0.019
$[c\text{-}Au_3(\mu_2\text{-}F)_3](B_3N_3H_6)$	−9.6	−0.132	−0.011	0.124
$[c\text{-}Au_3(\mu_2\text{-}F)_3](B_3N_3H_6)_2$	−8.9	−0.129	−0.007	0.063
$[c\text{-}Au_3(\mu_2\text{-}F)_3]_2(B_3N_3H_6)$	−9.0	−0.125	−0.012	0.136
$[c\text{-}Au_3(\mu_2\text{-}Cl)_3](B_3N_3H_6)$	−6.3	−0.110	−0.008	0.065
$[c\text{-}Au_3(\mu_2\text{-}Cl)_3](B_3N_3H_6)_2$	−6.5	−0.103	−0.003	0.016
$[c\text{-}Au_3(\mu_2\text{-}Cl)_3]_2(B_3N_3H_6)$	−5.7	−0.103	−0.008	0.070
$[c\text{-}Au_3(\mu_2\text{-}Br)_3](B_3N_3H_6)$	−5.9	−0.112	−0.007	0.046
$[c\text{-}Au_3(\mu_2\text{-}Br)_3](B_3N_3H_6)_2$	−6.3	−0.108	−0.003	0.023
$[c\text{-}Au_3(\mu_2\text{-}Br)_3]_2(B_3N_3H_6)$	−6.0	−0.114	−0.008	0.070
$[c\text{-}Au_3(\mu_2\text{-}I)_3](B_3N_3H_6)$	−5.2	−0.110	−0.008	0.027
$[c\text{-}Au_3(\mu_2\text{-}I)_3](B_3N_3H_6)_2$	−6.0	−0.113	−0.004	0.005
$[c\text{-}Au_3(\mu_2\text{-}I)_3]_2(B_3N_3H_6)$	−5.9	−0.119	−0.010	0.054

^{a}Dissociation energies, D_0 (in kcal/mol), are calculated for the adiabatic dissociation processes $[c\text{-}Au_3(\mu_2\text{-}X)_3](L) \rightarrow [c\text{-}Au_3(\mu_2\text{-}X)_3] + L$, $[c\text{-}Au_3(\mu_2\text{-}X)_3](L)_2 \rightarrow [c\text{-}Au_3(\mu_2\text{-}X)_3](L) + L$, and $[c\text{-}Au_3(\mu_2\text{-}X)_3]_2(L) \rightarrow [c\text{-}Au_3(\mu_2\text{-}X)_3](L) + [c\text{-}Au_3(\mu_2\text{-}X)_3]$, corrected for ZPE and BSSE errors. $^b q_{NCD}$ is the net charge donation.

Scheme 2

HOMO-18   HOMO-19   HOMO-31   HOMO-35   HOMO-39
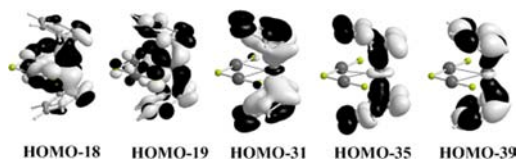
We also calculated the dissociation energies, D_0, for the adiabatic processes yielding the $c\text{-}Au_3(\mu_2\text{-}X)_3$ and L stacking participants in their ground states, corrected for ZPE and BSSE (Table 4) at the M05-2X/Def2-TZVPP level. Noteworthy, the estimated dissociation energies found in the range from −4.6 to −10.2 kcal/mol are much lower than the respective interaction energies, ΔE_{int}, calculated at the revPBE-D3/TZ2P level (Table 3)
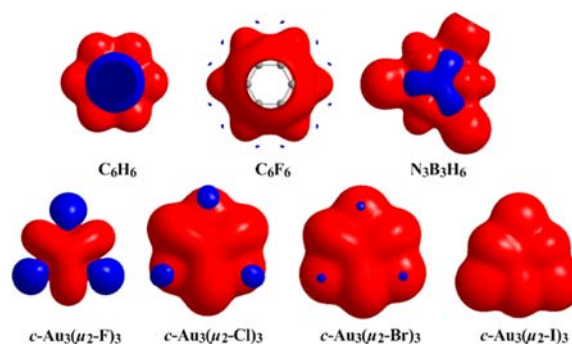
Figure 2. 3D contour plots of the MEP (positive and negative regions shown in red and blue, respectively) of the $c\text{-}Au_3(\mu_2\text{-}X)_3$ (X = F, Cl, Br, I) CTCs and the benzene, hexafluorobenzene, and borazine molecules calculated at the M05-2X/Def2-TZVPP level (isosurface value = 0.260 au).

employing the EDA method. These differences must come from the different theoretical methods employed and the fact that D_0 and ΔE_{int} correspond to adiabatic and diabatic dissociation processes, respectively. To test the performance of the M05-2X functional employed for calculation of the dissociation energies, D_0, of the $[c\text{-}Au_3(\mu_2\text{-}X)_3](L)$ (L = C_6H_6, C_6F_6, $B_3N_3H_6$) pff stacks we calculated the adiabatic dissociation energies for the $C_6H_6\cdots C_6H_6$, $C_6F_6\cdots C_6F_6$, and $C_6F_6\cdots C_6H_6$ stacks which were found to be 1.7, 3.3, and 4.8 kcal/mol, respectively. These values are in excellent agreement with the experimental value of 1.6 ± 0.2 kcal/mol for the $(C_6H_6)_2$ pff stacks[42] and the estimated MP2-(full)/6-31+G** value of 5.12 kcal/mol for the $(C_6H_6)(C_6F_6)$ pff stacks.[43]

The weak stacking interactions in the $[c\text{-}Au_3(\mu_2\text{-}X)_3](L)$ (L = C_6H_6, C_6F_6, $B_3N_3H_6$) pff stacks are clearly visualized as broad regions in real space by the 3D plots of the reduced density gradient (RDG). 3D plots of RDG for representative pff stacks and the $c\text{-}Au_3(\mu_2\text{-}X)_3$ CTCs are given in Figure 4. 3D plots of RDG for the remaining pff stacks are given in the Supporting Information (Figures S6−S8). For the sake of comparison, 3D plots of RDG for $C_6H_6\cdots C_6H_6$, $C_6F_6\cdots C_6F_6$, $C_6F_6\cdots C_6H_6$, $C_6H_6\cdots B_3N_3H_6$, and $C_6F_6\cdots B_3N_3H_6$ pff stacks have also been included in Figure 4.

In the $c\text{-}Au_3(\mu_2\text{-}X)_3$ CTCs there is an area of nonbonded overlap (steric repulsions) located at the centers of the Au_3 and the peripheral Au_2X rings. The nearly disc-shaped isosurfaces found at the middle of the Au−Au and Au−X bonds are characteristic of strong attractive interactions. In the $[c\text{-}Au_3(\mu_2\text{-}X)_3](L)$ pff stacks there are broad multiform RDG domains (concave surfaces with holes) in the region between the stacked molecules which characterize the weak noncovalent interactions. The isosurfaces show also nonbonded overlap (steric repulsions) within the six-membered rings of the ligands L. The same holds true for the $C_6H_6\cdots C_6H_6$, $C_6F_6\cdots C_6F_6$, $C_6F_6\cdots C_6H_6$, $C_6H_6\cdots B_3N_3H_6$, and $C_6F_6\cdots B_3N_3H_6$ pff stacks. It can be seen that the noncovalent interactions seem to be stronger in the regions between the peripheral atoms of the rings of the stacking participants. From the comparison of the RDG isosurfaces of the $[c\text{-}Au_3(\mu_2\text{-}X)_3](L)$ pff stacks with those of the L⋯L and L⋯L′ pff stacks the stronger aromatic interactions in the former than in the latter are immediately clear. Moreover, the appearance of small disc-shaped RDG domains (with deep green color) in the RDG isosurfaces of the $[c\text{-}Au_3(\mu_2\text{-}X)_3](L)$ pff stacks demonstrate the contribution of weak covalent (donor−acceptor) interactions to the aromatic
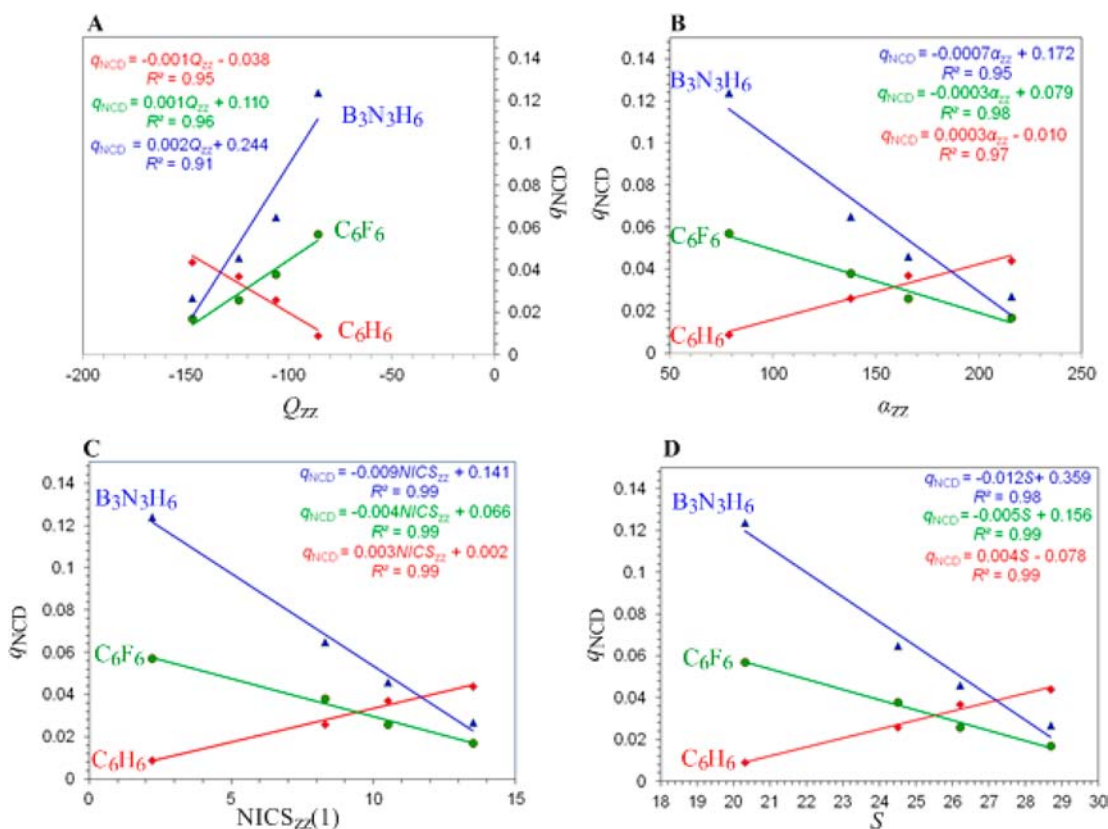
Figure 3. Relationships between the net charge donation (q_{NCD}) and the physical properties of the $c\text{-}Au_3(\mu_2\text{-}X)_3$ CTCs (Table 2); (A) zz tensor component of quadrupole moment, Q_{zz}; (B) zz tensor component of the polarizability, α_{zz}; (C) zz tensor component of the nucleus-independent chemical shift $NICS_{zz}(1)$ (1 Å above the corresponding ring center); (D) estimated surface area S computed at the M05-2X/Def2-TZVPP level.

interactions. Such interactions are not visualized on the RDG isosurfaces of the L···L and L···L′ **pff** stacks.

3.2. Magnetotropicity of the $[c\text{-}Au_3(\mu_2\text{-}X)_3]_n(L)_m$ (X = Halide; L = C_6H_6, C_6F_6, or $B_3N_3H_6$; n, $m \leq 2$) Binary Stacks. The magnetotropicity of the $[c\text{-}Au_3(\mu_2\text{-}X)_3]_n(L)_m$ (X = F, Cl, Br, I; L = C_6H_6, C_6F_6, or $B_3N_3H_6$; n, $m \leq 2$) binary stacks was evaluated by the $NICS_{zz}$-scan curves, which in conjunction with symmetry-based selection rules for the most significant $T_{x,y}$- and R_z-allowed transitions helped rationalize and predict the orbital type of aromaticity/antiaromaticity of the clusters.[44] Merino and co-workers[45] showed that $NICS_{zz}$ is equivalent to the z component of the induced magnetic field B_z^{ind} for an external field perpendicular to the ring, since the induced magnetic field $B^{ind}(R)$ is related to the shielding tensor at position R and the external magnetic field B^{ext} according to the equation $B^{ind}(R) = -\sigma(R)B^{ext}$. Accordingly, the $NICS_{zz}$-scan profiles are similar to the $B_z^{ind}(R)$-scan profiles. Notice that the z component of the induced magnetic field B_z^{ind} allows quantification of the magnetic response, thus being an analytical probe of electron delocalization in a wide range of molecules (aromatic, antiaromatic, and non-aromatic). Representative $NICS_{zz}$-scan profiles referring to the $[c\text{-}Au_3(\mu_2\text{-}Cl)_3]_n(L)_m$ (L = C_6H_6, C_6F_6, or $B_3N_3H_6$; n, $m \leq 2$) binary stacks are shown in Figure 5, while the $NICS_{zz}$-scan profiles for all binary stacks are given in the Supporting Information (Figures S9–S11). The most salient features of the $NICS_{zz}$-scan curves for all binary stacks and their "free-standing" $c\text{-}Au_3(\mu_2\text{-}X)_3$ and L stacking participants are compiled in Table 5.

It can be seen that the magnetic response of the Au_3 rings in the $c\text{-}Au_3(\mu_2\text{-}X)_3$ (X = F, Cl, Br, I) CTCs is paratropic (antiaromatic) in the ring planes. All $c\text{-}Au_3(\mu_2\text{-}X)_3$ (X = F, Cl,

Br, I) rings are long-range diatropic (aromatic) with relatively small minimum $NICS_{zz}(R)$ values of -4.2, -5.3, -5.6, and -5.7 ppm at 2.3, 2.5, 2.7, and 2.8 Å above and below the ring planes for the fluoro, chloro, bromo, and iodo derivatives, respectively. The $NICS_{zz}$-scan curves of the $c\text{-}Au_3(\mu_2\text{-}X)_3$ (X = F, Cl, Br, I) rings are typical for antiaromatic systems.

Let us first examine the magnetotropicity of the benzene stacks. In the $[c\text{-}Au_3(\mu_2\text{-}X)_3]_n(C_6H_6)_m$ (X = F, Cl, Br, I) binary stacks, except $[c\text{-}Au_3(\mu_2\text{-}F)_3](C_6H_6)_2$, the interacting inorganic and organic (C_6H_6, C_6F_6, or $B_3N_3H_6$) rings keep the main features of the individual magnetic response behavior. Thus, in these binary stacks the inorganic ring is still paratropic (antiaromatic) at the ring centers but exhibiting lower paratropicity with respect to the "free-standing" $c\text{-}Au_3(\mu_2\text{-}X)_3$ CTCs. The decrease of the magnetic antiaromaticity at the centers of the inorganic rings, as it is expressed by the $NICS_{zz}(0)$ values, is higher in the 1:2 **pff** stacks (lowered by 10.4–14.1 ppm) and almost similar in the 1:1 and 2:1 **pff** stacks (lowered by 5.6–8.5 ppm). The decrease of the magnetic antiaromaticity at the centers of the inorganic rings could be due to the fact that the ghost Bq atoms are located into the shielding cone of the benzene stacking participant. Reduction of NICS values has previously been observed in stacked aromatic rings as in [2.2]paracyclophane or in the benzene and xylene dimers and was attributed to the coupling between, i.e., the sum of, the magnetic fields created by the electron current densities of the two rings one placed above the other.[46] The benzene ring in the $[c\text{-}Au_3(\mu_2\text{-}X)_3]_n(C_6H_6)_m$ (X = F, Cl, Br, I) binary stacks, except $[c\text{-}Au_3(\mu_2\text{-}F)_3](C_6H_6)_2$, shows the typical $NICS_{zz}$-scan profile of the "free" benzene but with higher
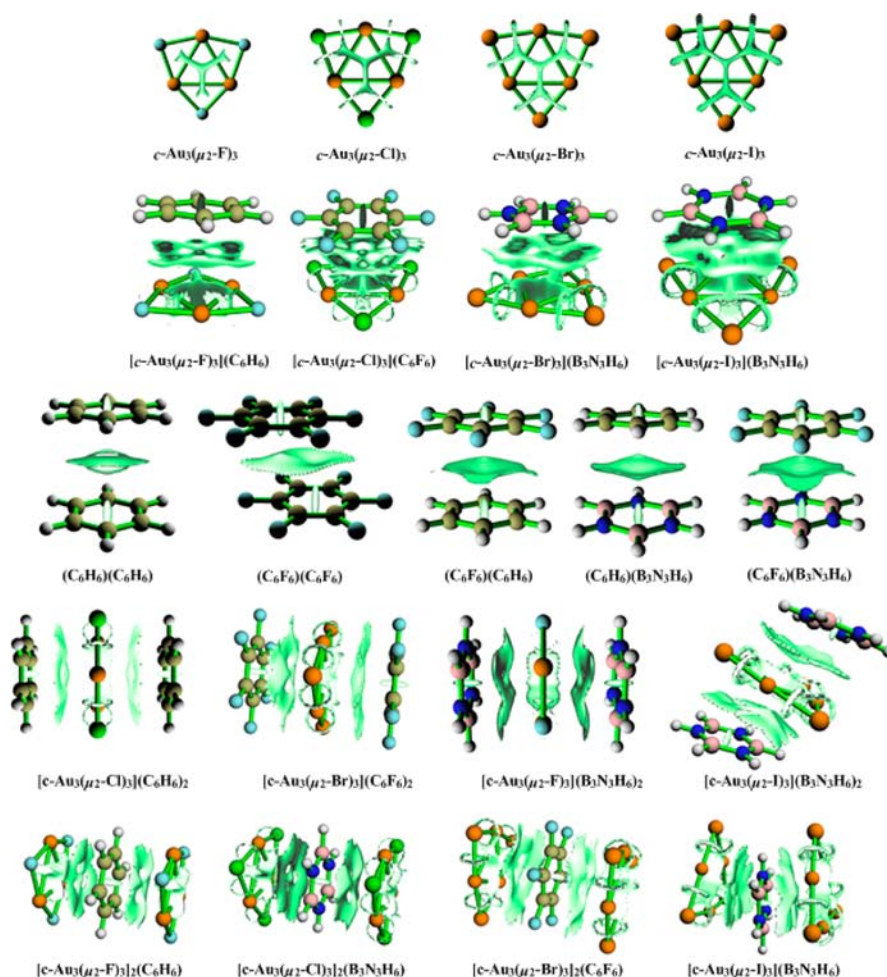
Figure 4. 3D plots of the reduced density gradient, RDG (isosurface = 0.500), for representative $[c\text{-}Au_3(\mu_2\text{-}X)_3]_n(L)_m$ (X = halide; L = C_6H_6, C_6F_6, or $B_3N_3H_6$; n, $m \leq 2$), the $c\text{-}Au_3(\mu_2\text{-}X)_3$ CTCs, and L···L and L···L′ **pff** stacks computed at the M05-2X/Def2-TZVPP level.
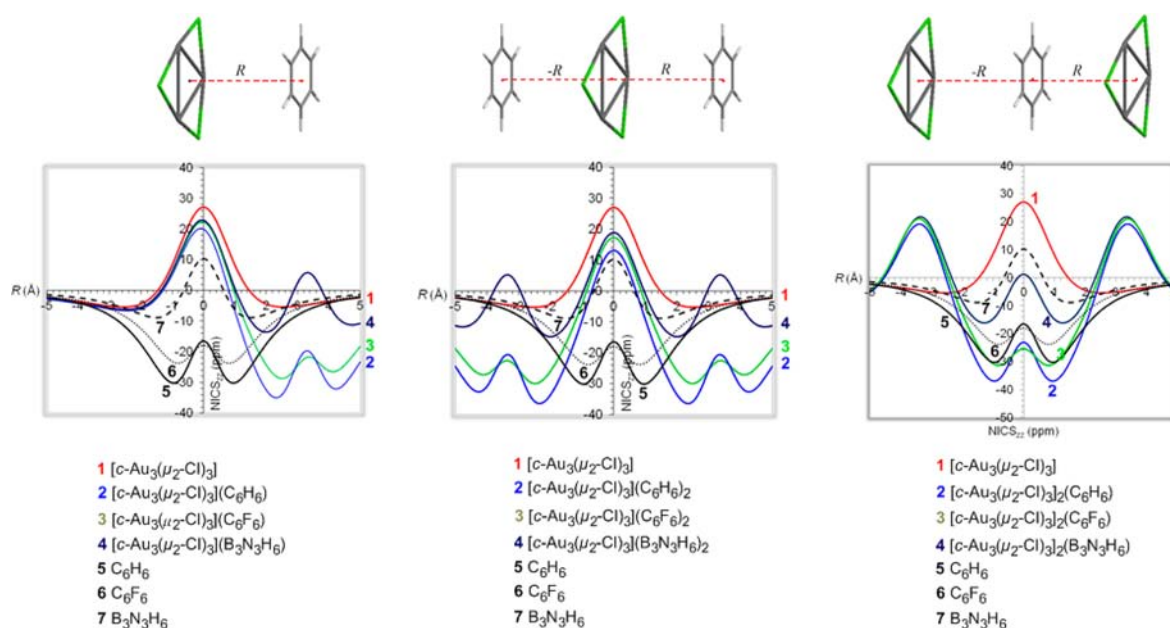
Figure 5. NICS$_{zz}$-scan profiles of the of the $[c\text{-}Au_3(\mu_2\text{-}Cl)_3]_n(L)_m$ (L = C_6H_6, C_6F_6, or $B_3N_3H_6$; n, $m \leq 2$) binary stacks computed at the GIAO-B3LYP/Def2-TZVPP level.

Table 5. $NICS_{zz}(0)$ and $NICS_{zz}(\pm 1)$ Values (in ppm) Calculated at the Inorganic and Organic Ring Centers and at Distances 1 Å Inward and Outward of the Inorganic and Organic Ring Planes for the $[c\text{-}Au_3(\mu_2\text{-}X)_3]_n(L)_m$ (X = F, Cl, Br, I; L = C_6H_6, C_6F_6, or $B_3N_3H_6$; n, m ≤ 2) Binary Stacks Computed at the GIAO-B3LYP/Def2-TZVPP Level

| | $c\text{-}Au_3(\mu_2\text{-}X)_3$ | | L | |
compound	$NICS_{zz}(0)$	$NICS_{zz}(\pm 1)$	$NICS_{zz}(0)$	$NICS_{zz}(\pm 1)$
C_6H_6			−16.5	−30.1
$[c\text{-}Au_3(\mu_2\text{-}F)_3](C_6H_6)$	3.7	−1.2 (−14.7)^a	−19.0	−31.5 (−33.6)
$[c\text{-}Au_3(\mu_2\text{-}Cl)_3](C_6H_6)$	19.9	5.3 (−6.9)	−19.7	−31.9 (−34.9)
$[c\text{-}Au_3(\mu_2\text{-}Br)_3](C_6H_6)$	24.5	7.7 (−4.2)	−20.0	−32.2 (−34.9)
$[c\text{-}Au_3(\mu_2\text{-}I)_3](C_6H_6)$	30.0	11.2 (−0.3)	−20.0	−32.3 (−34.9)
$[c\text{-}Au_3F_2(\mu_2\text{-}F)(\eta^3\text{-}C_6H_6)_2]$	−2.5	−15.5	−1.1	1.1 (−3.4)
$[c\text{-}Au_3(\mu_2\text{-}Cl)_3](C_6H_6)_2$	13.1	−9.4	−20.7	−32.6 (−36.4)
$[c\text{-}Au_3(\mu_2\text{-}Br)_3](C_6H_6)_2$	18.4	−6.2	−20.8	−32.7 (−36.4)
$[c\text{-}Au_3(\mu_2\text{-}I)_3](C_6H_6)_2$	25.2	−1.5	−20.8	−32.9 (−36.1)
$[c\text{-}Au_3(\mu_2\text{-}F)_3]_2(C_6H_6)$	3.2	−1.8 (−15.3)	−21.1	−35.1
$[c\text{-}Au_3(\mu_2\text{-}Cl)_3]_2(C_6H_6)$	18.9	4.3 (−7.8)	−23.1	−36.9
$[c\text{-}Au_3(\mu_2\text{-}Br)_3]_2(C_6H_6)$	23.0	7.5 (−6.9)	−23.5	−37.2
$[c\text{-}Au_3(\mu_2\text{-}I)_3]_2(C_6H_6)$	28.5	10.2 (2.3)	−23.7	−37.2
C_6F_6			−18.0	−23.2
$[c\text{-}Au_3(\mu_2\text{-}F)_3](C_6F_6)$	6.9	−0.6 (−8.2)	−20.5	−24.7 (−27.1)
$[c\text{-}Au_3(\mu_2\text{-}Cl)_3](C_6F_6)$	22.2	5.8 (−1.4)	−21.8	−25.4 (−27.9)
$[c\text{-}Au_3(\mu_2\text{-}Br)_3](C_6F_6)$	26.5	8.2 (1.2)	−22.0	−25.9 (−28.4)
$[c\text{-}Au_3(\mu_2\text{-}I)_3](C_6F_6)$	31.1	11.4 (4.6)	−22.4	−26.2 (−28.5)
$[c\text{-}Au_3(\mu_2\text{-}F)_3](C_6F_6)_2$	1.9	−11.2	−21.5	−25.4 (−28.8)
$[c\text{-}Au_3(\mu_2\text{-}Cl)_3](C_6F_6)_2$	17.2	−4.1	−22.6	−26.5 (−29.3)
$[c\text{-}Au_3(\mu_2\text{-}Br)_3](C_6F_6)_2$	21.8	−1.3	−22.8	−26.5 (−29.6)
$[c\text{-}Au_3(\mu_2\text{-}I)_3](C_6F_6)_2$	26.7	2.4	−23.1	−26.7 (−29.5)
$[c\text{-}Au_3(\mu_2\text{-}F)_3]_2(C_6F_6)$	6.1	−1.1 (−9.4)	−23.0	−28.6
$[c\text{-}Au_3(\mu_2\text{-}Cl)_3]_2(C_6F_6)$	20.8	5.8 (−4.4)	−25.4	−30.7
$[c\text{-}Au_3(\mu_2\text{-}Br)_3]_2(C_6F_6)$	25.2	6.7 (−0.1)	−26.1	−31.2
$[c\text{-}Au_3(\mu_2\text{-}I)_3]_2(C_6F_6)$	29.6	8.9 (4.2)	−26.7	−31.5
$B_3N_3H_6$			10.3	−6.3
$[c\text{-}Au_3(\mu_2\text{-}F)_3](B_3N_3H_6)$	7.5	−0.1 (−5.6)	7.1	−8.5 (−10.1)
$[c\text{-}Au_3(\mu_2\text{-}Cl)_3](B_3N_3H_6)$	22.8	6.4 (0.7)	5.8	−9.1 (−11.9)
$[c\text{-}Au_3(\mu_2\text{-}Br)_3](B_3N_3H_6)$	27.3	8.8 (3.0)	5.3	−9.0 (−12.5)
$[c\text{-}Au_3(\mu_2\text{-}I)_3](B_3N_3H_6)$	32.5	12.1 (6.4)	5.1	−9.5 (−12.3)
$[c\text{-}Au_3(\mu_2\text{-}F)_3](B_3N_3H_6)_2$	3.6	−7.9	6.1	−9.2 (−11.6)
$[c\text{-}Au_3(\mu_2\text{-}Cl)_3](B_3N_3H_6)_2$	18.9	−1.2	2.9	−6.3 (−14.6)
$[c\text{-}Au_3(\mu_2\text{-}Br)_3](B_3N_3H_6)_2$	24.1	2.1	0.0	−9.4 (−12.9)
$[c\text{-}Au_3(\mu_2\text{-}I)_3](B_3N_3H_6)_2$	29.9	6.0	5.4	−9.6 (−13.3)
$[c\text{-}Au_3(\mu_2\text{-}F)_3]_2(B_3N_3H_6)$	6.8	−1.0 (−6.2)	4.0	−12.3
$[c\text{-}Au_3(\mu_2\text{-}Cl)_3]_2(B_3N_3H_6)$	21.7	5.6 (−1.1)	1.2	−14.8
$[c\text{-}Au_3(\mu_2\text{-}Br)_3]_2(B_3N_3H_6)$	26.2	7.9 (1.7)	1.5	−15.3
$[c\text{-}Au_3(\mu_2\text{-}I)_3]_2(B_3N_3H_6)$	31.1	11.0 (4.7)	1.0	−16.0
$c\text{-}Au_3(\mu_2\text{-}F)_3$	11.6	2.2		
$c\text{-}Au_3(\mu_2\text{-}Cl)_3$	27.0	8.3		
$c\text{-}Au_3(\mu_2\text{-}Br)_3$	31.1	10.5		
$c\text{-}Au_3(\mu_2\text{-}I)_3$	35.6	13.5		

^{a}Figures in parentheses are the $NICS_{zz}(1)$ values at a point inward the respective ring plane.

minimum $NICS_{zz}(0)$ and $NICS_{zz}(1)$ values from −19.0 to −23.7 and −31.7 to −37.2 ppm at the ring center and 1 Å below the ring plane, respectively. The point 1 Å below the benzene ring plane is located in the space between the inorganic and the benzene ring planes. Noteworthy, the minimum $NICS_{zz}$ values occur at 2.1−2.5 Å inward the Au_3 ring plane in the $[c\text{-}Au_3(\mu_2\text{-}X)_3]_n(C_6H_6)_m$ (X = F, Cl, Br, I; n, m ≤ 2) **pff** stacks. The observed enhancement of the diatropicity of the benzene rings, particularly in the region between the interacting rings (compare the $NICS_{zz}$-scan curves of the $[c\text{-}Au_3(\mu_2\text{-}X)_3](C_6H_6)$ **pff** stacks and the "free" benzene shown in Figure 5), could be attributed to superposition of the diamagnetic ring currents

(coupling of the induced magnetic fields) of the stacked inorganic and benzene rings. The enhancement of the diatropicity of the benzene and metallic rings in their **pff** stacks was further corroborated by calculating the induced magnetic fields B_z^{ind} assuming an external magnetic field of $|B^{ext}| = 1$ T. In this case the unit of the induced magnetic field is 1 μT, which is equivalent to 1 ppm of the shielding tensor.[45] The increase of local aromaticty in the superimposed rings indicated by the computed B_z^{ind} given in the Supporting Information (Table S2) is caused by the coupling of the induced magnetic fields.[46] The estimated $\Delta B_z^{ind}(0)$ $[\Delta B_z^{ind}(\pm 1)]$ values for the inorganic and organic rings were found in the range 3.1−13.9 μT [7.1−17.7 μT]

and 2.5–10.3 μT [3.5–9.7 μT], respectively. Noteworthy, the increase of local aromaticity caused by the coupling of the induced magnetic fields is more pronounced in the inorganic (Au_3X_3) than in the organic (L) rings. In the peculiar bent structure of $[c\text{-}Au_3(\mu_2\text{-}F)_3](C_6H_6)_2$ the η^3-bonding mode of the benzene ligands to one of the gold(I) atoms disrupts the delocalization on the coordinated benzene ligands, rendering them nonaromatic (see the $NICS_{zz}(0)$ and $NICS_{zz}(\pm 1)$ values given in Table 5).

All $[c\text{-}Au_3(\mu_2\text{-}X)_3]_n(C_6F_6)_m$ (X = F, Cl, Br, I) binary stacks show analogous $NICS_{zz}$-scan profiles with the following main features: The inorganic rings are paratropic (antiaromatic) at the ring centers. At a distance of 1 Å inward the Au_3 ring the $NICS_{zz}(1)$ values (from −11.4 to 4.6 ppm) are indicative for practically nonaromatic rings, while the $NICS_{zz}(-1)$ values (from −0.6 to 11.4 ppm) at a distance 1 Å outward the Au_3 ring plane are indicative for paratropic ring currents outward the Au_3 ring plane. The hexafluorobenzene ring in all $[c\text{-}Au_3(\mu_2\text{-}X)_3]_n(C_6F_6)_m$ (X = F, Cl, Br, I) binary stacks show the typical

$NICS_{zz}$-scan profile of the "free" C_6F_6 ring but with enhanced diatropicity particularly in the space between the stacking participants (compare the $NICS_{zz}$-scan curves of the $[c\text{-}Au_3(\mu_2\text{-}X)_3](C_6F_6)_2$ **pff** stacks and the "free" C_6F_6 shown in Figure 5). The enhancement of the diatropicity in the region between the interacting rings could also be due to superposition of the individual diamagnetic ring currents (coupling of the induced magnetic fields) of the stacked inorganic and organic ring systems.

The magnetic response of the $[c\text{-}Au_3(\mu_2\text{-}X)_3]_n(B_3N_3H_6)_m$ (X = F, Cl, Br, I) binary stacks, as it is imprinted on the $NICS_{zz}$-scan profiles, can be analyzed as follows: The interacting inorganic rings exhibit similar magnetotropic patterns to those of the corresponding benzene and hexafluorobenzene stacks. They are paratropic (antiaromatic) at the ring centers and practically nonaromatic at a distance of 1 Å above and below the ring plane. The borazine ring in all $[c\text{-}Au_3(\mu_2\text{-}X)_3]_n(B_3N_3H_6)_m$ (X = F, Cl, Br, I) binary stacks shows the typical $NICS_{zz}$-scan profile of the "free" $B_3N_3H_6$ ring but again with enhanced diatropicity particularly in the space between the stacking participants (Figure 5). Once again the enhancement of the diatropicity in the region between the interacting rings is due to the superposition of the individual diamagnetic ring currents (coupling of the induced magnetic fields) of the stacked inorganic and organic ring systems.

3.3. Possible Applications in Organic Electronics. It is well established that charge carrier mobility, i.e., the hole and electron transport is of paramount importance in designing molecular devices, e.g., thin-film transistors (OTFTs), organic light-emitting diodes (OLEDs), and plastic photovoltaic cells. The charge motion occurs by hopping, and the electron hopping process is described by Marcus theory.[47] The rate constant for electron transfer occurring between two neighboring molecules stacked together is proportional to the square of the so-called charge transfer integral, t_{12}.[48] Given that there is negligible or no covalent interaction between the stacked molecules, the charge transfer integral, t_{12} could then be calculated based on the energy split in the dimer model (ESID). According to the ESID method,

Table 6. Charge Transfer Integrals for Hole, t_{12}^h, and Electron Transport, t_{12}^e, for $[c\text{-}Au_3(\mu_2\text{-}X)_3](L)$ (X = F, Cl, Br, I; L = C_6H_6, C_6F_6, or $B_3N_3H_6$; n, $m \leq 2$) 1:1 Binary Stacks Calculated at the TDDFT-PBE0/Def2-TZVPP Level

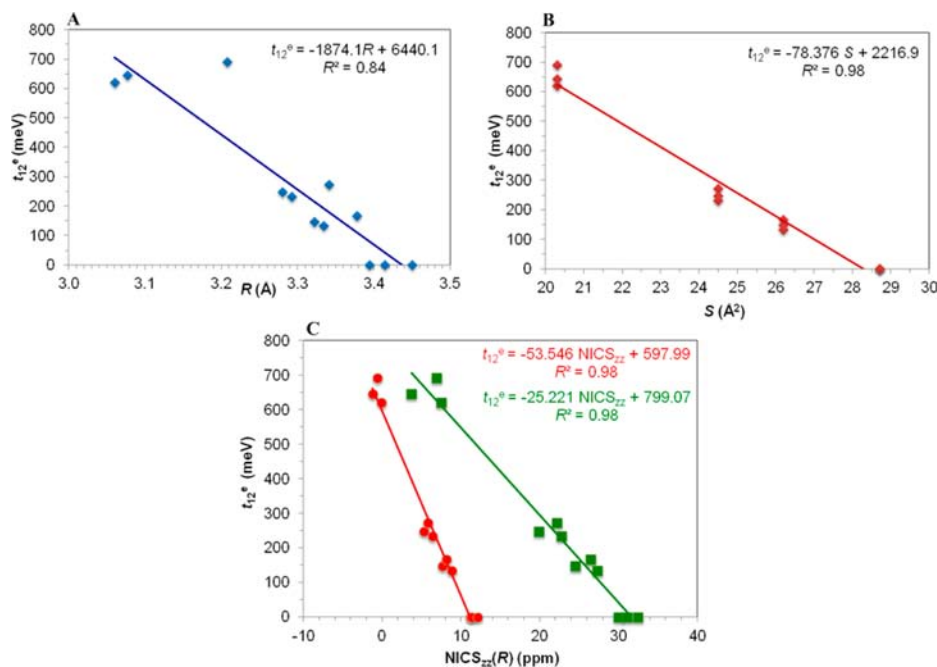| dimer	t_{12}^h (meV)	t_{12}^e (meV)
$[c\text{-}Au_3(\mu_2\text{-}F)_3](C_6H_6)$	0.5	645.0
$[c\text{-}Au_3(\mu_2\text{-}Cl)_3](C_6H_6)$	0.0	247.5
$[c\text{-}Au_3(\mu_2\text{-}Br)_3](C_6H_6)$	0.0	147.5
$[c\text{-}Au_3(\mu_2\text{-}I)_3](C_6H_6)$	0.0	0.0
$[c\text{-}Au_3(\mu_2\text{-}F)_3](C_6F_6)$	0.5	692.0
$[c\text{-}Au_3(\mu_2\text{-}Cl)_3](C_6F_6)$	0.0	273.0
$[c\text{-}Au_3(\mu_2\text{-}Br)_3](C_6F_6)$	0.0	167.0
$[c\text{-}Au_3(\mu_2\text{-}I)_3](C_6F_6)$	0.0	0.0
$[c\text{-}Au_3(\mu_2\text{-}F)_3](B_3N_3H_6)$	0.0	621.0
$[c\text{-}Au_3(\mu_2\text{-}Cl)_3](B_3N_3H_6)$	0.5	233.0
$[c\text{-}Au_3(\mu_2\text{-}Br)_3](B_3N_3H_6)$	0.5	133.0
$[c\text{-}Au_3(\mu_2\text{-}I)_3](B_3N_3H_6)$	0.0	0.0

Figure 6. Linear correlation between t_{12}^e and the intermolecular distance, R (A), cluster surface area (B), and $NICS_{zz}$ (red circles and green squares refer to the outward $NICS_{zz}(-1)$ and $NICS_{zz}(0)$, respectively) (C) found for the $[c\text{-}Au_3(\mu_2\text{-}X)_3](L)$ 1:1 binary stacks.

the charge transfer integral for hole [electron] transfer is generally taken as one-half the energetic difference of the HOMO and HOMO-1 [LUMO and LUMO+1] energy levels of a molecular dimer. The charge transfer integrals for hole, t_{12}^h, and electron transport, t_{12}^e, calculated for $[c\text{-Au}_3(\mu_2\text{-X})_3](\text{L})$ (X = F, Cl, Br, I; L = C_6H_6, C_6F_6, or $\text{B}_3\text{N}_3\text{H}_6$; $n, m \leq 2$) 1:1 binary stacks at the TDDFT-PBE0/Def2-TZVPP level are given in Table 6.

Inspection of Table 6 reveals that t_{12}^h values are zero or near zero, indicating that hole transport in these dimers is expected to be very limited. On the other hand, t_{12}^e values are quite large (130−700 meV), rendering them excellent materials for use in electron-channel organic conductors. Notice that to date most organic semiconductors have been found to be hole-channel charge transporters (based on materials with relatively high t_{12}^h).[49] In order to gain further insight to the factors related to the charge transfer integrals we set out to explore if there are any correlations with other structural, electronic, or magnetic parameters also calculated for the $[c\text{-Au}_3(\mu_2\text{-X})_3](\text{L})$ 1:1 binary stacks. In Figure 6 are given the best linear correlations between t_{12}^e and various other parameters.

A good linear correlation is observed between the metallic cluster−L intermolecular distance, r, and t_{12}^e. The latter gives an excellent linear correlation with the surface area of the metallic cluster. Next, in Figure 6 are given the linear correlation of t_{12}^e with the magnetic criterion of aromaticity NICS_{zz} at various points. Surprisingly, t_{12}^e gives excellent linear correlations with both outward $\text{NICS}_{zz}(-1)$ and $\text{NICS}_{zz}(0)$ of the dimers. The excellent linear correlation between t_{12}^e and $\text{NICS}_{zz}(-1)$ may be indirectly related to the effect of amount of electron density on the t_{12}^e value. However, t_{12}^e does not correlate with the inward $\text{NICS}_{zz}(1)$, illustrating that the decrease of the NICS_{zz} in the inner region is associated only to magnetic couplings with neighboring superimposed rings and not to significant electron density changes in the rings. These findings are in line with those reported by Poater et al.[46a] for [2.2]paracyclophane or in the benzene and xylene dimers.

4. CONCLUSIONS

Our main findings can be summarized as follows.

(i) The molecular and electronic structures, stabilities, bonding features, and magnetotropicity of the columnar binary stacks with general formula $[c\text{-Au}_3(\mu_2\text{-X})_3]_n(\text{L})_m$ (X = halide; L = C_6H_6, C_6F_6, or $\text{B}_3\text{N}_3\text{H}_6$; $n, m \leq 2$) have been investigated by DFT calculations at the M05-2X/Def2-TZVPP level of theory. In all binary stacks, with only a few exceptions, the plane of the alternating $c\text{-Au}_3(\mu_2\text{-X})_3$ and L (C_6H_6, C_6F_6, $\text{B}_3\text{N}_3\text{H}_6$) stacking participants adopts an almost parallel face-to-face (**pff**) orientation. The observed trends in the intermolecular distances R in the $[c\text{-Au}_3(\mu_2\text{-X})_3]_n(\text{L})_m$ (X = halide; L = C_6H_6, C_6F_6, $\text{B}_3\text{N}_3\text{H}_6$; $n, m \leq 2$) columnar binary stacks are explained by the diverse aromatic interactions characterizing the stacks, since the three L ligands and the $c\text{-Au}_3(\mu_2\text{-X})_3$ CTCs exhibit diverse physical properties such as the zz tensor components of quadrupole moment, Q_{zz}, polarizability, α_{zz}, nucleus-independent chemical shift, $\text{NICS}_{zz}(1)$, along with the molecular electrostatic potential, MEP(0), and surface area (S), which are important determinants of the aromatic interactions.

(ii) The interplay of electrostatics, charge transfer, and dispersion forces contributing to the interaction energies in the 1:1, 1:2, and 2:1 binary stacks of the $c\text{-Au}_3(\mu_2\text{-X})_3$ (X = F, Cl, Br, I) clusters with benzene, hexafluorobenzene, or borazine was investigated by employing a multitude of theoretical techniques such as charge and energy decomposition analysis (CDA and EDA), natural bond orbital (NBO) population analysis, as well as molecular electrostatic potential (MEP) calculations. It was found that the dominant term in the aromatic (stacking) interactions arises mainly from dispersion and electrostatic forces, while the contribution of covalent interactions is predicted to be small. According to CDA results, very small charge transfer from the L stacking participants toward the $c\text{-Au}_3(\mu_2\text{-X})_3$ clusters takes place. EDA and CDA results point out that maximizing electrostatic attraction may be an effective way to obtain favorably stacked columns between $c\text{-Au}_3(\mu_2\text{-X})_3$ CTCs and various arenes.

(iii) Important linear correlations of the interaction energy, ΔE_{int}, and its components (ΔE_{disp}, ΔE_{elstat}, ΔE_{orb}, and ΔE_{Pauli}) with the aforementioned calculated physical properties were established. The most important finding is the excellent linear relationship between ΔE_{int} and the $\text{NICS}_{zz}(1)$, indicating that ΔE_{int} is also affected by the coupling of the induced magnetic fields of the interacting stacking participants.

(iv) The magnetotropicity of the binary stacks was evaluated by the NICS_{zz}-scan curves and the estimated z component of the induced magnetic field B_z^{ind}. Noteworthy, the interacting inorganic and organic rings keep their magnetic response properties in the clusters but show an appreciable enhancement of the diatropic (aromatic) character due to superposition of the diamagnetic ring currents (coupling of the induced magnetic fields) of the stacked inorganic and benzene rings.

(v) Large charge transfer integrals for electron transport, t_{12}^e, are calculated for most of the $[c\text{-Au}_3(\mu_2\text{-X})_3](\text{L})$ 1:1 binary stacks, rendering them promising candidates for use as electron channel semiconductors in organic electronics.

■ ASSOCIATED CONTENT

S Supporting Information

Complete author list for ref 22; equilibrium geometries of the $[c\text{-Au}_3(\mu_2\text{-X})_3]_n(\text{L})_m$ (X = halide; L = C_6H_6, C_6F_6, $\text{B}_3\text{N}_3\text{H}_6$; $n, m \leq 2$) binary stacks; relationships between the interaction energy (ΔE_{int}) and the calculated physical properties of the $[c\text{-Au}_3(\mu_2\text{-X})_3]_n(\text{L})_m$ columnar binary stacks; 3D plots of the reduced density gradient, RDG, for the $[c\text{-Au}_3(\mu_2\text{-X})_3]_n(\text{L})_m$ binary stacks; NICS_{zz}-scan profiles of the $[c\text{-Au}_3(\mu_2\text{-X})_3]_n(\text{L})_m$ columnar binary stacks; linear relationships of ΔE_{int} and its components (ΔE_{disp}, ΔE_{elstat}, ΔE_{orb}, and ΔE_{Pauli}) with calculated physical properties related to dispersion and electrostatic forces; enhancement of the induced magnetic fields B_z^{ind} upon stacking of the superimposed rings; Cartesian coordinates and energetic data. This material is available free of charge via the Internet at http://pubs.acs.org.

■ AUTHOR INFORMATION

Corresponding Author

*E-mail: attsipis@uoi.gr.

Notes

The authors declare no competing financial interest.

■ REFERENCES

(1) (a) Ma, J. C.; Daugherty, D. A. *Chem. Rev.* **1997**, *97*, 1303−1324. (b) McGaughey, G. B.; Gagné, M.; Rappé, A. K. *J. Biol. Chem.* **1998**, *273*, 15458−15463. (c) Kannan, N.; Vishveshwara, S. *Protein Eng.* **2000**, *13*, 753−761. (d) Meyer, E. A.; Castellano, R. K.; Diederich, F. *Angew. Chem., Int. Ed. Engl.* **2003**, *42*, 1210−1250. (e) Kaplan, I. G. *Intermolecular Interactions*; J. Wiley & Sons: Chichester, U.K., 2006. (f) Schottel, B. L.; Chifotides, H. T.; Dunbar, K. R. *Chem. Soc. Rev.* **2008**, *37*, 68−83. (g) Schneider, H.-J. *Angew. Chem., Int. Ed. Engl.* **2009**, *48*, 3924−3977. (h) Salonen, L. M.; Ellermann, M.; Diederich, F. *Angew. Chem., Int. Ed. Engl.* **2011**, *50*, 4808−4842. (i) Watt, M.; Hardebeck, L. K. E.; Kirkpatrick, C. C.; Lewis, M. *J. Am. Chem. Soc.* **2011**, *133*, 3854−3862. (j) Bloom, J. W. G.; Wheeler, S. E. *Angew. Chem., Int. Ed. Engl.* **2011**, *50*, 7847−7849.

(2) (a) Tsuzuki, S.; Tsuzuki, S.; Uchimaru, T.; Mikami, M. *J. Phys. Chem. A* **2006**, *110*, 2027−2033. (b) Cockroft, S. L.; Hunter, C. A. *Chem. Soc. Rev.* **2007**, *36*, 172−188. (c) Sherrill, C. D.; Takatani, T.; Hohenstein, E. G. *J. Phys. Chem. A* **2009**, *113*, 10146−10159. (d) Mati, I. K.; Cockroft, S. L. *Chem. Soc. Rev.* **2010**, *39*, 4195−4205.

(3) Murahashi, T.; Fujimoto, M.; Oka, M.; Hashimoto, Y.; Uemura, T.; Tatsumi, Y.; Nakao, Y.; Ikeda, A.; Sakaki, S.; Kurosawa, H. *Science* **2006**, *313*, 1104−1107.

(4) Muñiz, J.; Sansores, L. E.; Martínez, A.; Salcedo, R. *J. Mol. Model.* **2008**, *14*, 417−425.

(5) Tekarli, S. M.; Cundari, T. R.; Omary, M. A. *J. Am. Chem. Soc.* **2008**, *130*, 1669−1675.

(6) Tsipis, A. C.; Stalikas, A. V. *Inorg. Chem.* **2012**, *51*, 2541−2559.

(7) Burini, A.; Mohamed, A. A.; Fackler, J. P., Jr. *Comments Inorg. Chem.* **2003**, *24*, 253−280.

(8) Schmidbaur, H. *Chem. Soc. Rev.* **1995**, *24*, 391−400.

(9) Mingos, D. M. P. *J. Chem. Soc., Dalton Trans.* **1996**, *5*, 561−566.

(10) Van Zyl, W. E.; López-de-Luzuriaga, J. M.; Fackler, J. P., Jr *J. Mol. Struct.* **2000**, *516*, 99−106.

(11) Schmidbaur, H. *Gold Bull.* **1990**, *23*, 11−21.

(12) (a) Pyykkö, P. *Chem. Rev.* **1997**, *97*, 597−636. (b) Sansores, L. E.; Salcedo, R.; Flores, H.; Martínez, A. *J. Mol. Struct. (THEOCHEM)* **2000**, *530*, 125−129. (c) Muñiz, J.; Sansores, L. E.; Martínez, A.; Salcedo, R. *J. Mol. Struct. (THEOCHEM)* **2007**, *820*, 141−147. (d) Sansores, L. E.; Salcedo, R.; Martínez, A. *J. Mol. Struct. (THEOCHEM)* **2004**, *677*, 145−151. (e) Li, J.; Pyykkö, P. *Chem. Phys. Lett.* **1992**, *197*, 586−590. (f) Pyykkö, P.; Li, L.; Runeberg, N. *Chem. Phys. Lett.* **1994**, *218*, 133−138. (g) Pyykkö, P. *Angew. Chem., Int. Ed. Engl.* **2002**, *41*, 3573−3578. (h) Schwerdtfeger, P. *Angew. Chem., Int. Ed. Engl.* **2003**, *42*, 1892−1895.

(13) (a) Omary, M. A.; Mohamad, A. A.; Rawashdeh-Omary, M. A.; Fackler, J. P., Jr. *Coord. Chem. Rev.* **2005**, *249*, 1372−1381 and references therein. (b) Olmstead, M. M.; Jiang, F.; Attar, S.; Balch, A. L. *J. Am. Chem. Soc.* **2001**, *123*, 3260−3267. (c) Rawashdeh-Omary, M. A.; Omary, M. A.; Fackler, J. P., Jr. *J. Am. Chem. Soc.* **2001**, *123*, 9689−9691. (d) Burini, A.; Fackler, J. P., Jr.; Galassi, R.; Grant, T. A.; Omary, M. A.; Rawashdeh-Omary, M. A.; Pietroni, B. R.; Staples, R. J. *J. Am. Chem. Soc.* **2000**, *122*, 11264−11265. (e) Omary, M. A.; Mohamad, A. A.; Rawashdeh-Omary.; Gonser, M. W. A.; Elbjeirami, O.; Grimes, T.; Cundari, T. A. *Inorg. Chem.* **2005**, *44*, 8200−8210.

(14) (a) Mendizabal, F.; Burgos, D.; Olea-Azar, C. *Chem. Phys. Let.* **2008**, *463*, 272−277. (b) Mendizabal, F. *Int. J. Quantum Chem.* **2010**, *110*, 1279−1286.

(15) Fayet, P.; Granzer, F.; Hegenbart, G.; Moisar, E.; Pischel, B.; Wöste, L. *Z. Phys. D: At. Mol. Clusters* **1986**, *3*, 299−302.

(16) (a) Bertolus, M.; Brenner, V.; Millie, P. *Eur. Phys. J.* **2000**, *D11*, 387−394. (b) L'Hermite, J.-M.; Rabilloud, F.; Labastie, P.; Spiegelman, F. *Eur. Phys. J.* **2001**, *D16*, 77−80. (c) L'Hermite, J.-M.; Rabilloud, F.; Marcou, L.; Labastie, P. *Eur. Phys. J.* **2001**, *D14*, 323−330.

(17) (a) Wong, C.-H.; Schomaker, V. *J. Phys. Chem.* **1957**, *61*, 358−360. (b) Klemperer, W.; Rice, S. T.; Berry, R. S. *J. Am. Chem. Soc.* **1957**, *79*, 1810−1811. (c) Guido, M.; Balducci, G.; Gigli, G.; Spoliti, M. *J. Chem. Phys.* **1971**, *55*, 4566−4572. (d) Martin, T. P.; Kakizaki, A. *J. Chem. Phys.* **1984**, *80*, 3956−3961. (e) Martin, T. P.; Schaber, H. J.

Chem. Phys. **1980**, *73*, 3541−3546. (f) Hargittai, M.; Schwerdtfeger, P.; Réffy, B.; Brown, R. *Chem.—Eur. J.* **2003**, *9*, 327−333. (g) Rabilloud, F.; Bonhomee, O.; L' Hermite, J. M.; Labastie, P. *Chem. Phys. Let.* **2008**, *454*, 153−157. (h) Yin, Y.-H.; Chen, H.-S.; Song, Y. *J. Mol. Struct. (THEOCHEM)* **2010**, *959*, 30−34. (i) Rabilloud, F.; Spiegelmann, F.; Heully, J. L. *J. Chem. Phys.* **1999**, *111*, 8925−8933. (j) Zhang, H.; Schelly, Z. A.; Marynick, D. S. *J. Phys. Chem. A* **2000**, *104*, 6287−6294. (k) Rabilloud, F.; Spiegelmann, F.; L' Hermite, J. M.; Labastie, P. *J. Chem. Phys.* **2001**, *114*, 289−305. (l) Kodaira, T.; Ikeda, T.; Takeo, H. *Eur. Phys. J. D* **1999**, *9*, 601. (m) Kovács, A.; Konings, R. J. M. *J. Mol. Struct.* **2002**, *643*, 155−160.

(18) Rabilloud, F. *J. Comput. Chem.* **2012**, *33*, 2083−2091.

(19) Rabilloud, F. *J. Phys. Chem. A* **2012**, *116*, 3474−3480.

(20) (a) Zhao, Y.; Schultz, N. E.; Truhlar, D. G. *J. Chem. Theor. Comput.* **2006**, *2*, 364−382. (b) Zhao, Y.; Schultz, N. E.; Truhlar, D. G. *J. Chem. Theor. Comput.* **2006**, *2*, 1009−1018.

(21) Weigend, F.; Ahlrichs, R. *Phys. Chem. Chem. Phys.* **2005**, *7*, 3297−3305.

(22) Frisch, M. J.; et al. *Gaussian 09*, Revision A.02; Gaussian, Inc.: Wallingford, CT, 2009.

(23) Boys, S. F.; Bernardi, F. *Mol. Phys.* **1970**, *19*, 553−566.

(24) Simon, S.; Duran, M.; Dannenberg, J. J. *J. Chem. Phys.* **1996**, *105*, 11024−11031.

(25) (a) Reed, A. E.; Curtiss, L. A.; Weinhold, F. *Chem. Rev.* **1988**, *88*, 899−926. (b) Weinhold, F. In *The Encyclopedia of Computational Chemistry*; Schleyer, P. v. R., Ed.; John Wiley & Sons: Chichester, 1998; pp 1792−1811.

(26) (a) Ditchfield, R. *Mol. Phys.* **1974**, *27*, 789. (b) Gauss, J. *J. Chem. Phys.* **1993**, *99*, 3629−3643.

(27) (a) Becke, A. D. *J. Chem. Phys.* **1992**, *96*, 2155−2160. (b) Becke, A. D. *J. Chem. Phys.* **1993**, *98*, 5648−5652. (c) Lee, C.; Yang, W.; Parr, R. G. *Phys. Rev. Lett.* **1998**, *B 37*, 785−789.

(28) Schleyer, P. v. R.; Maerker, C.; Dransfeld, A.; Jiao, H.; Hommes, N. J. *J. Am. Chem. Soc.* **1996**, *118*, 6317−6318.

(29) (a) Daprich, S.; Frenking, G. *J. Phys. Chem.* **1995**, *99*, 9352−9362. (b) Frenking, G.; Frohlich, N. *Chem. Rev.* **2000**, *100*, 717−774.

(30) (a) Gorelsky, S. I.; Ghosh, S.; Solomon, E. I. *J. Am. Chem. Soc.* **2006**, *128*, 278−290. (b) Gorelsky, S. I. *AOMIX*; Department of Chemistry, York University: Toronto, ON, 2011; http://www.sg-chem.net. (c) Gorelsky, S. I.; Lever, A. B. P. *J. Organomet. Chem.* **2001**, *635*, 187−196.

(31) (a) Morokuma, K. *J. Chem. Phys.* **1971**, *55*, 1236−1244. (b) Morokuma, K. *Acc. Chem. Res.* **1977**, *10*, 294−300. (c) Ziegler, T.; Rauk, A. *Theor. Chim. Acta* **1977**, *46*, 1−10.

(32) *ADF2010.01 SCM*, Theoretical Chemistry, Vrije Universiteit: Amsterdam, The Netherlands.

(33) (a) Chang, C.; Pelissier, M.; Durand, Ph. *Phys. Scr.* **1986**, *34*, 394−404. (b) Heully, J.-L.; Lindgren, I.; Lindroth, E.; Lundquist, S.; Martensson-Pendrill, A.-M. *J. Phys. B* **1986**, *19*, 2799−2815. (c) Van Lenthe, E.; Baerends, E. J.; Snijders, J. G. *J. Chem. Phys.* **1993**, *99*, 4597−4610. (d) Van Lenthe, E.; Baerends, E. J.; Snijders, J. G. *J. Chem. Phys.* **1996**, *105*, 6505−6516. (e) Van Lenthe, E.; Van Leeuwen, R.; Baerends, E. J.; Snijders, J. G. *Int. J. Quantum Chem.* **1996**, *57*, 281−293.

(34) (a) Grimme, S.; Antony, J.; Ehrich, S.; Krieg, H. *J. Chem. Phys.* **2010**, *132*, 154104−154122. (b) Goerigk, L.; Grimme, S. *Phys. Chem. Chem. Phys.* **2011**, *13*, 6670−6688.

(35) Baerends, E. J.; Ellis, D. E.; Roos, P. *Chem. Phys.* **1973**, *2*, 41−51.

(36) Lu, T.; Chen, F. *J. Comput. Chem.* **2012**, *33*, 580−592.

(37) (a) Rosenstock, H. M.; Sites, J. R.; Walton, J. R.; Baldock, R. *J. Chem. Phys.* **1955**, *23*, 2442. (b) Graber, P.; Weil, K. G. *Ber. Bunsen-Ges. Phys. Chem.* **1973**, *77*, 507. (c) Bernauer, O.; Weil, K. G. *Ber. Bunsen-Ges. Phys. Chem.* **1974**, *78*, 1339. (d) Pittermann, U.; Weil, K. G. *Ber. Bunsen-Ges. Phys. Chem.* **1980**, *84*, 542.

(38) Ruivo, D.; Pereiro, A. B.; Esperança, J. M. S. S.; Canongia Lopes, J. N.; Rebelo, L. P. N. *J. Phys. Chem. B* **2010**, *114*, 12589−12596.

(39) Dennis, G. R.; Ritchie, G. L. D. *J. Phys. Chem.* **1993**, *97*, 8403−8409.

(40) (a) Hunter, C. A. *J. Mol. Biol.* **1993**, *230*, 1025−1054. (b) Cozi, F.; Cinquini, M.; Annuziata, R.; Siegel, J. S. *J. Am. Chem. Soc.* **1993**, *115*, 5330−5331. (c) Hunter, C. A. *Chem. Soc. Rev.* **1994**, 101−118. (d) Jorgensen, W. L.; Severance, D. L. *J. Am. Chem. Soc.* **1990**, *112*, 4768−4774. (e) Guckian, K. M.; Schweitzer, B. A.; Ren, R. X.-F.; Sheils, C. J.; Tahmassebi, D. C.; Kool, E. T. *J. Am. Chem. Soc.* **2000**, *122*, 2213−2222.

(41) (a) Wheeler, S. E.; Houk, K. N. *J. Am. Chem. Soc.* **2008**, *130*, 10854−10855. (b) Wheeler, S. E. *J. Am. Chem. Soc.* **2011**, *133*, 10262−10274.

(42) Hobza, P.; Selzle, H. L.; Schlag, E. W. *J. Am. Chem. Soc.* **1994**, *116*, 3500−3506.

(43) Gung, B. W.; Amicangelo, J. C. *J. Org. Chem.* **2006**, *71*, 9261−9270.

(44) (a) Tsipis, A. C.; Depastas, I. G.; Tsipis, C. A. *Symmetry* **2010**, *2*, 284−319 and references therein. (b) Tsipis, C. A. *Struct. Bonding (Berlin)* **2010**, *136*, 217 and references therein.

(45) (a) Merino, G.; Heine, T.; Seifert, G. *Chem.—Eur. J.* **2004**, *10*, 4367−4371. (b) Islas, R.; Heine, T.; Merino, G. *Acc. Chem. Res.* **2012**, *45*, 215−228.

(46) (a) Poater, J.; Bofill, J. M.; Alemany, P.; Solá, M. *J. Org. Chem.* **2006**, *71*, 1700−1702. (b) Islas, R.; Martínez-Guajardo, G.; Jiménez-Halla, J.; Oscar, C.; Solá, M.; Merino, G. *J. Chem. Theor. Comput.* **2010**, *6*, 1131−1135.

(47) (a) Marcus, R. A. *J. Chem. Phys.* **1956**, *24*, 979−989. (b) Marcus, R. A. *Can. J. Chem.* **1959**, *37*, 155−163. (c) Marcus, R. A. *J. Phys. Chem.* **1963**, *67*, 853−857.

(48) Koh, S. E.; Risko, C.; Da Silva Filho, D. A.; Kwon, O.; Facchetti, A.; Brédas, J.-L.; Marks, T. J.; Ratner, M. A. *Adv. Funct. Mater.* **2008**, *18*, 332−340.

(49) (a) Mitzi, D. B.; Dimitrakopoulos, C. D.; Kosbar, L. L. *Chem. Mater.* **2001**, *13*, 3728−3740. (b) Kraft, A. *ChemPhysChem* **2001**, *2*, 163−165. (c) Dimitrakopoulos, C. D.; Malenfant, P. R. L. *Adv. Mater.* **2002**, *14*, 99−117. (d) Afzali, A.; Dimitrakopoulos, C. D.; Breen, T. L. *J. Am. Chem. Soc.* **2002**, *124*, 8812−8813. (e) Ponomarenko, S. A.; Kirchmeyer, S.; Elschner, A.; Huisman, B. H.; Karbach, A.; Drechsler, D. *Adv. Funct. Mater.* **2003**, *13*, 591−596. (f) Kunugi, Y.; Takimiya, K.; Yamane, K.; Yamashita, K.; Aso, Y.; Otsubo, T. *Chem. Mater.* **2003**, *15*, 6−7. (g) Meng, H.; Bendikov, M.; Mitchell, G.; Helgeson, R.; Wudl, F.; Bao, Z.; Siegrist, T.; Kloc, C.; Chen, C. H. *Adv. Mater.* **2003**, *15*, 1090−1093. (h) Videlot, C.; Ackermann, J.; Blanchard, P.; Raimundo, J. M.; Frere, P.; Allain, M.; De Bettignies, R.; Levillain, E.; Roncali. *Adv. Mater.* **2003**, *15*, 306−310.